Chapter VII

Ca and Sr co-doped ceria and its nanocomposites

This chapter is divided into two sections. Section 1 describes the effect of co-doping of Ca and Sr on the physical, structural and electrical properties of ceria. The composition which shows the highest conductivity has been chosen for the nanocomposites. Section 2 describes the effect of carbonates content $(Li_{0.52}Na_{0.48})_2CO_3$ on the physical, thermal, structural and electrical properties of Ca and Sr co-doped ceria.

7.1 Ca and Sr Co-Doped Ceria

7.1.1 Introduction

Ceria doped with alkaline earth oxides such as CaO [Blumenthal et al. (1967); Arai et al. (1986)] and SrO [Blumenthal et al. (1976); Yahiro et al. (1986)] has been studied extensively for application in IT-SOFCs. Electrical conductivity of CaO and SrO doped ceria is much higher than that of undoped ceria. The highest conductivity has been found in the composition $Ce_{0.90}Ca_{0.10}O_{1.90}$ by Shing et al. (2011) which is $\sim 10^{-3}$ S/cm at 600 ^{o}C. Yamashita et al. (1995) found that the composition $Ce_{0.90}Ca_{0.10}O_{1.90}$ has the highest conductivity $\sim 10^{-2}$ S/cm at 600 ^{o}C. Banerjee et al. (2008) studied the electrical properties of the system, $Ce_{1-x}Ca_xO_{2-\delta}$ $(0.05 \leq x \leq 0.20)$ prepared by a mixed fuel process followed by sintering at 1250 ^{o}C. They found that the composition, $Ce_{0.80}Ca_{0.20}O_{1.80}$ exhibits the highest conductivity (1.29×10^{-2} S/cm) at 600 ^{o}C.

Compositions in the system, $Ce_{1-x}Ca_xO_{2-\delta}$ with $0.05 \leq x \leq 0.20$ have been prepared by auto-combustion method by us and characterized. $Ce_{0.95}Ca_{0.05}O_{1.95}$ exhibits the maximum conductivity in this system. Composition exhibiting maximum conductivity in this system ($Ce_{1-x}Ca_xO_{2-\delta}$) has been reported to be different by different authors. This may be due to minor changes in the purity of raw materials and mainly changes in the processing conditions.

Co-doping of ceria has been found to be very effective approach for enhancement of the conductivity [Holtappels et al. (2000); Tuller et al. (2000); Etshell et al. (1970); Rickert et al. (1982)]. Most of these compounds contain one rare earth

element as a constituent. In the present investigations, effect of co-doping has been studied using Sr as a co-dopant in the composition $Ce_{0.95}Ca_{0.05}O_{1.95}$ which exhibits the maximum conductivity in our investigation as mentioned above.

Co-doping with Sr in singly doped ceria with a rare earth element has been reported to enhance its conductivity [Tsung et al. (2007); Ciotera et al. (2009); Zheng et al. (2009); Ramesh et al. (2009)]. In order to explore cheaper solid electrolyte for IT-SOFCs, a few samples of ceria co-doped with Ca and Sr in the system $Ce_{0.95-x}Ca_{0.05}Sr_xO_{2-\delta}$ [(x=0.0, CCO5), (x=0.01, CC5S1), (x=0.02, CC5S2) and (x=0.03, CC5S3)] have been synthesized and characterized.

7.1.2 Results and Discussion

(a) Thermal analysis

DTA/TGA plots of the as prepared ash of the composition, CCO5 is shown in Fig. 7.1. In TGA curve, a weight loss has been observed in a single step in the temperature range 70-300 °C. This is ascribed to the evaporation of absorbed moisture and burning of some organic residues. The total weight loss in the sample is 3 wt% (starting weight of the sample was 13.5 mg). In the DTA curve, one endothermic peak has been observed which corresponds to the weight loss observed in the TGA. There is no exo or endothermic peak observed beyond 300 °C. Based on this result, all the samples in this system were calcined at 600 °C for 4 hrs.

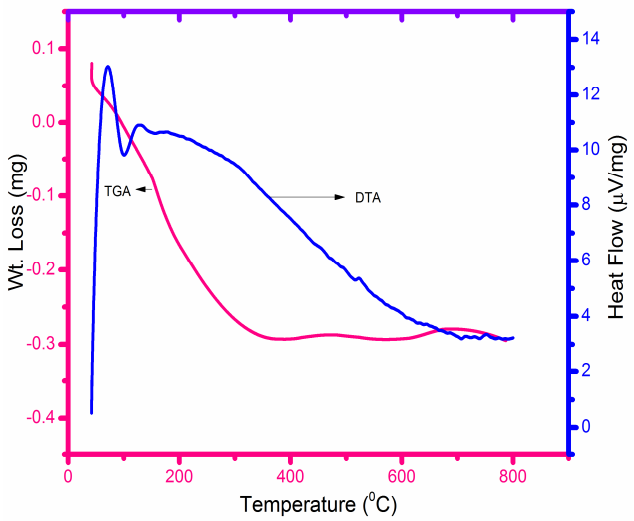

Fig. 7.1 DTA/TGA plots of the prepared ash of composition CCO5

(b) Crystal structure and phases

Powder X-ray diffraction patterns of all the calcined and sintered samples are recorded. All the samples are single phase having cubic fluorite structure similar to ceria. Diffraction patterns are indexed on the basis of fluorite structure similar to CeO_2 using JCPDS file no. 43-1002. XRD patterns for the calcined samples are similar to those obtained after sintering except that the diffraction lines become sharp. This is due to grain growth during sintering. The average crystallite size, D of the calcined powder calculated from X-ray line broadening using Scherrer's formula is given in Table. 7.1. Fig. 7.2 shows X-ray diffraction patterns of all the sintered samples in the system $Ce_{0.95-x}Ca_{0.05}Sr_xO_{1.95-x}$.

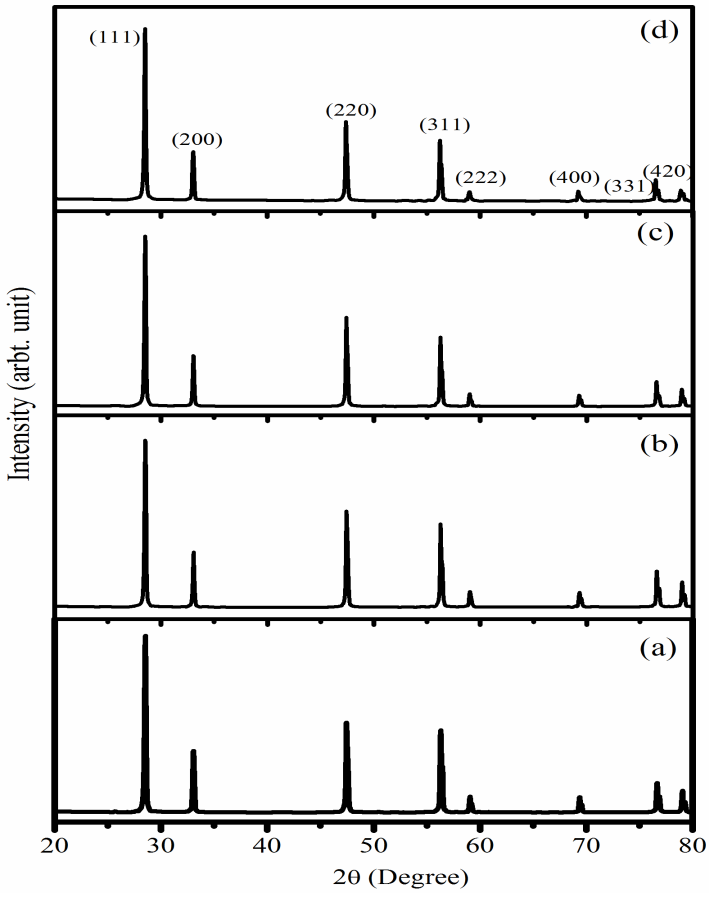

Fig. 7.2 Powder X-ray diffraction patterns of various compositions (a) CCO5 (b) CC5S1 (c) CC5S2 (d) CC5S3 sintered at 1350 °C

Characteristic lines of the constituent oxides are not observed in the diffraction patterns. There is a slight shift in 2θ values from the corresponding 2θ values of the composition CCO5. Lattice parameter of all the samples is given in Table. 7.1. Lattice parameter is found to increase with strontium content because the ionic radius of Sr^{2+} (1.26 Á) is larger than that of Ce^{4+} (0.97 Á). Density of the sintered pellets of all the samples determined by Archimedes principle is more than 97 % of the theoretical value (Table. 7.1).

Table. 7.1 Crystallite size, lattice parameter and % theoretical density of compositions in the system $Ce_{0.95-x}Ca_{0.05}Sr_xO_{1.95-x}$

S. No.	x	Sample code	Crystallite size (nm)	Lattice parameter (Å)	% TD
1.	0.0	CCO5	20	5.4120+/-0.0003	97.0
2.	0.01	CC5S1	21	5.4174+/-0.0002	98.3
3.	0.02	CC5S2	18	5.4192+/-0.0002	98.5
4.	0.03	CC5S3	23	5.4201+/-0.0006	97.5

(c) Microstructure

Fig. 7.3 shows SEM micrographs of all the sintered samples. Micrographs of the all samples show well-defined grains separated by the grain boundaries. All the samples have grains with varying size. Average grain size of the compositions with x = 0.00, 0.01, 0.02, and 0.03 determined by linear intercept method as well as 'ImageJ' software is approx. 2.0, 2.8, 2.5, and 2.1 μm respectively. It is observed from Fig. 7.3 that average grain size increases for the composition, CC5S1. Beyond x = 0.01, the average grain size decreases. This may be due to segregation of Sr^{2+} at grain boundaries due to elastic strain arising out of size mismatch between Sr^{2+} (1.26 Å) and Ce^{4+} (0.97 Å). EDS of the compositions, CCO5 and CC5S2 at three different points is shown in the Figs. 7.4 & 7.5 respectively. It can be seen from Fig. 7.4 that the spectrum at three points is almost the same except that a second phase containing

Si is present at the grain boundary and the triple point. Fig. 7.5 (spectrum of CC5S2) shows that Si is present at the triple point only. There is no Si present at the grain boundary. It may be due to scavenging effect of Sr. Due to large size of Sr^{2+} (1.26 Å), it may react with Si present at the grain boundary to form some silicate phases. These phases may segregate at the triple point leaving grain boundaries clean. The exact composition of these phases needs to be confirmed by STEM combined with EDXM and EELS [Gerhardt et al. (1986)].

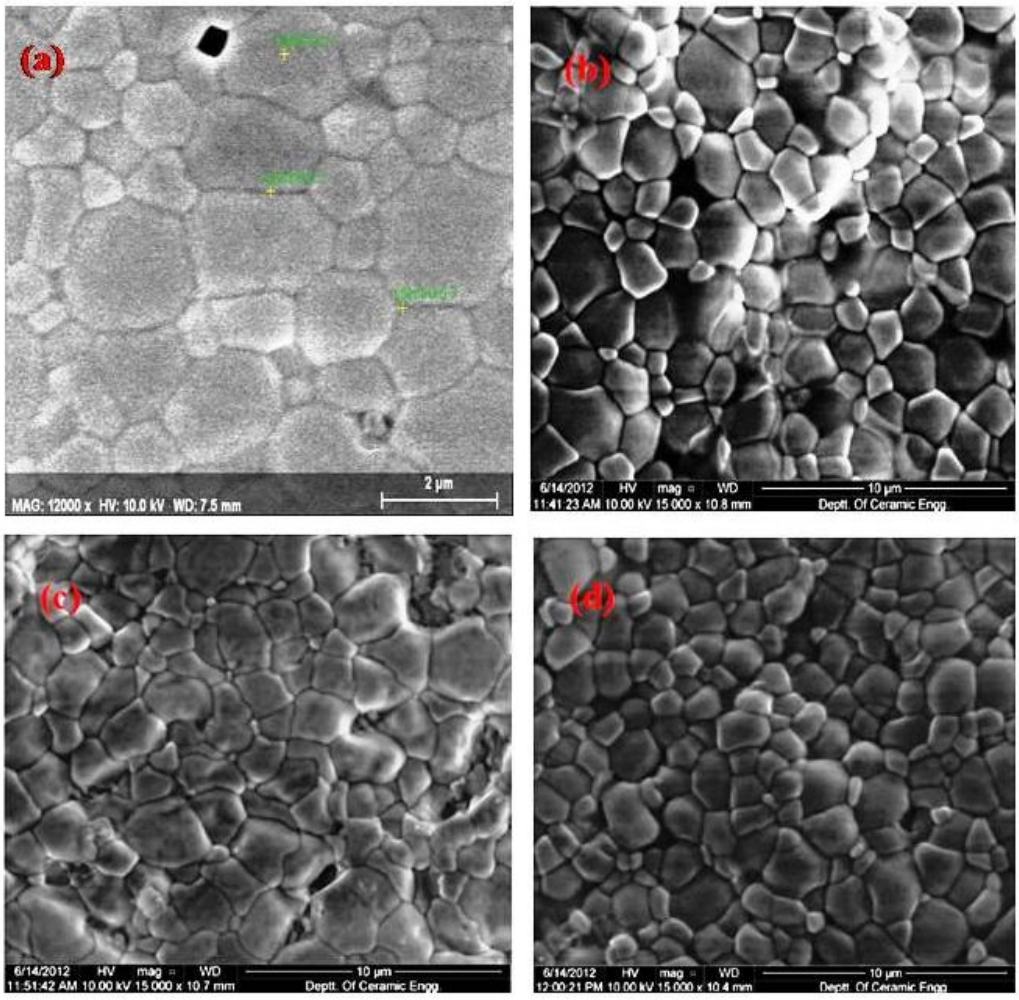

Fig. 7.3 SEM micrographs of the sintered samples of compositions (a) CCO5 (b) CC5S1 (c) CC5S2 (d) CC5S3

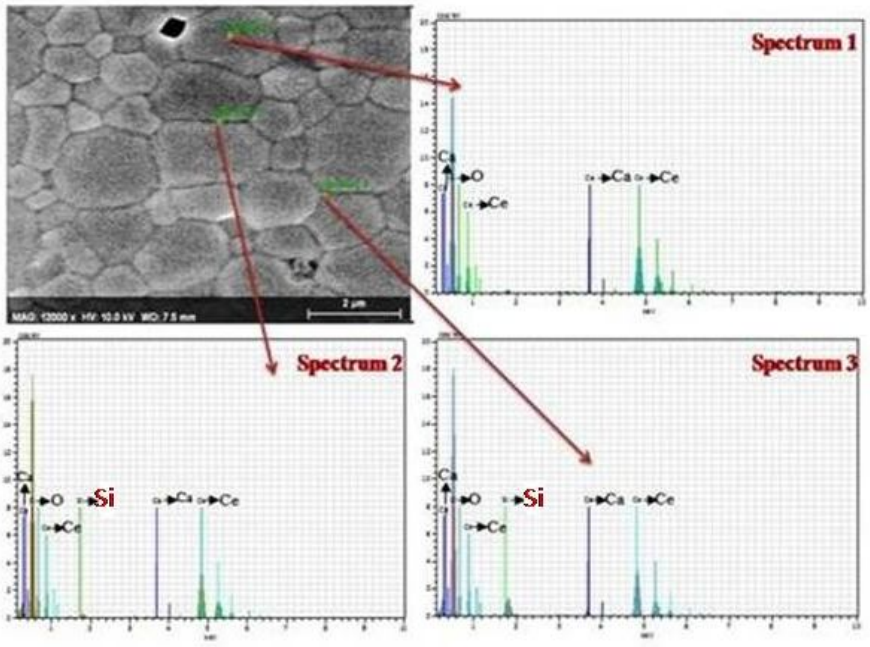

Fig. 7.4 EDS of the composition CCO5 at three different points: Spectrum1 (in the grain), Spectrum 2 (at the grain boundary) and Spectrum 3 (at the triple point)

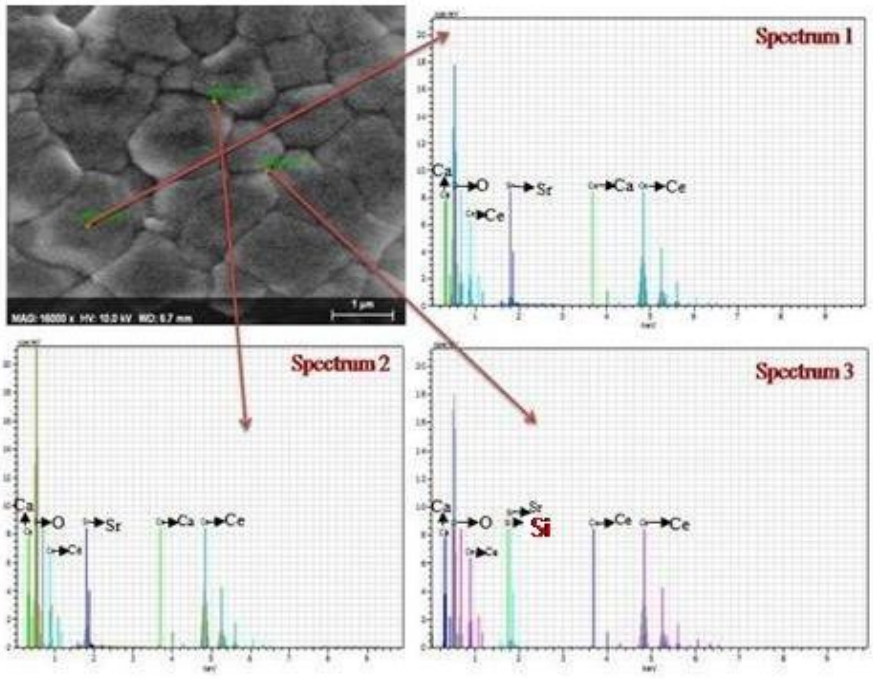

Fig. 7.5 EDS of the composition CC5S2 at three different points: Spectrum1 (in the grain), Spectrum 2 (at the grain boundary) and Spectrum 3 (at triple point)

(c) Electrical conductivity

Complex plane impedance plots of the compositions CCO5, CC5S1, CC5S2 and CC5S3 are shown in Figs. 7.6-7.9. For the composition, CCO5, three depressed distinct arcs have been observed in the temperature range 200-300 °C. The arc in the highest frequency region and passing through the origin is ascribed to the contribution of the grains to the total resistance. Arc in the intermediate frequency range corresponds to the contribution of the grain boundaries and the arc in the lowest frequency range corresponds to the electrode/electrolyte interface polarization. Due to shifting of the relaxation frequency of polarization processes towards higher side with increase in the temperature, the arc due to the grains disappears after 300 °C. The arc due to the grain boundaries disappears above 450 °C. Only the electrode arc has been observed at temperature > 450 °C. The grains and grain boundaries arcs are associated with the capacitances in the pF (10^{-10}-10^{-12}) and nF (10^{-7}-10^{-9}) ranges respectively. It determined from the relation $2\pi f_{max}RC = 1$, where f_{max} is the frequency at the highest point of the arc, R is the resistance and C is the capacitance of a particular contribution.

In the case of composition, CC5S1 three depressed arcs have been observed in the temperature range 200-300 °C. The arcs due to the grains and the grain boundaries disappear above 300 and 475 °C respectively.

Impedance plots were fitted to an equivalent circuit (as given in the Figs. 7.6-7.9) to determine the resistance of the grains and the grain boundaries. The sum of the resistance of the grains and the grain boundaries is equal to the total resistance of the sample. Therefore, only the arcs of the grains and the grain boundaries are fitted. At higher temperatures, the intercept on real Z' axis on higher frequency side of the electrode arc is taken as total resistance of the sample.

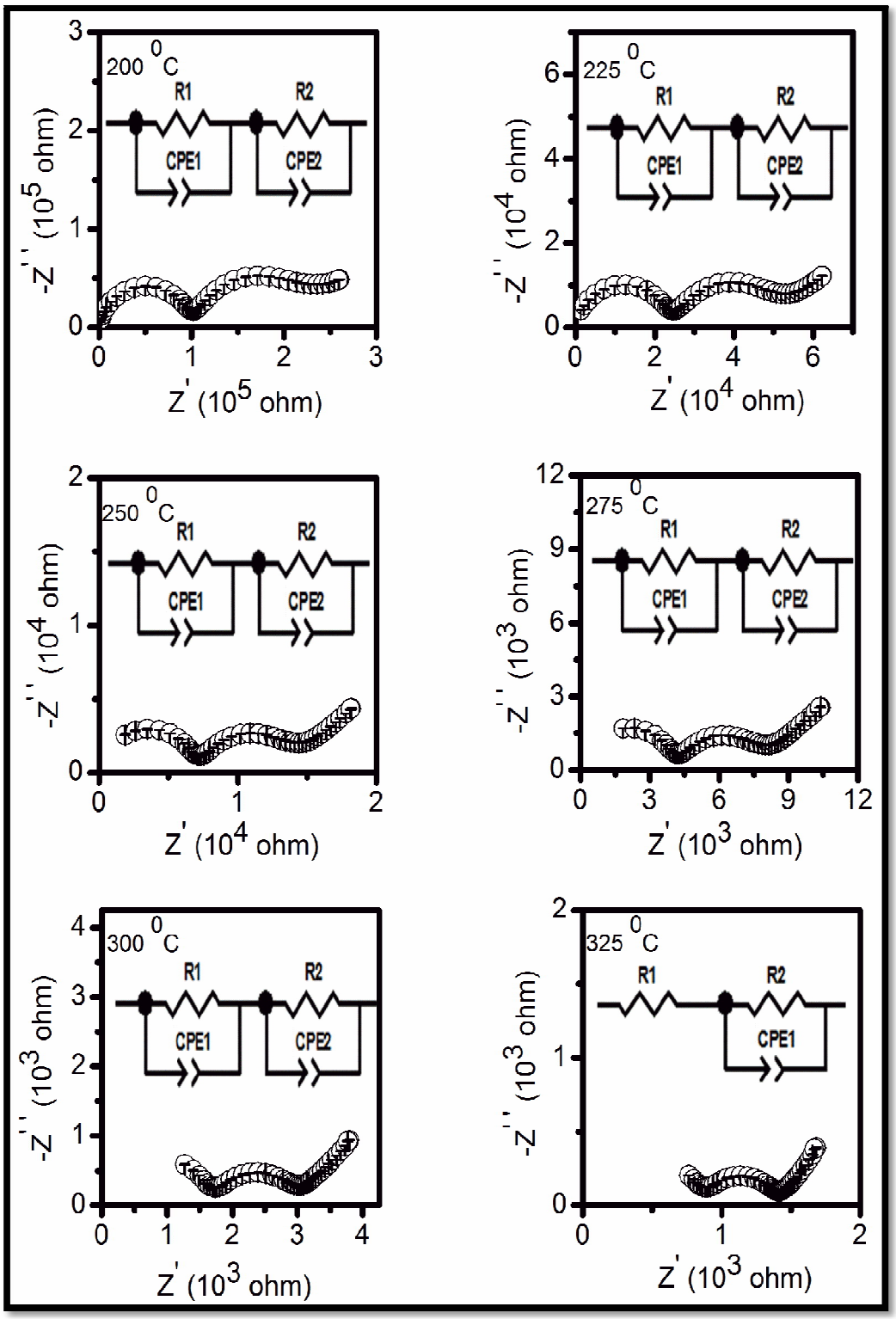

Fig. 7.6 Complex plane impedance plots of the composition CCO5 at different temperatures

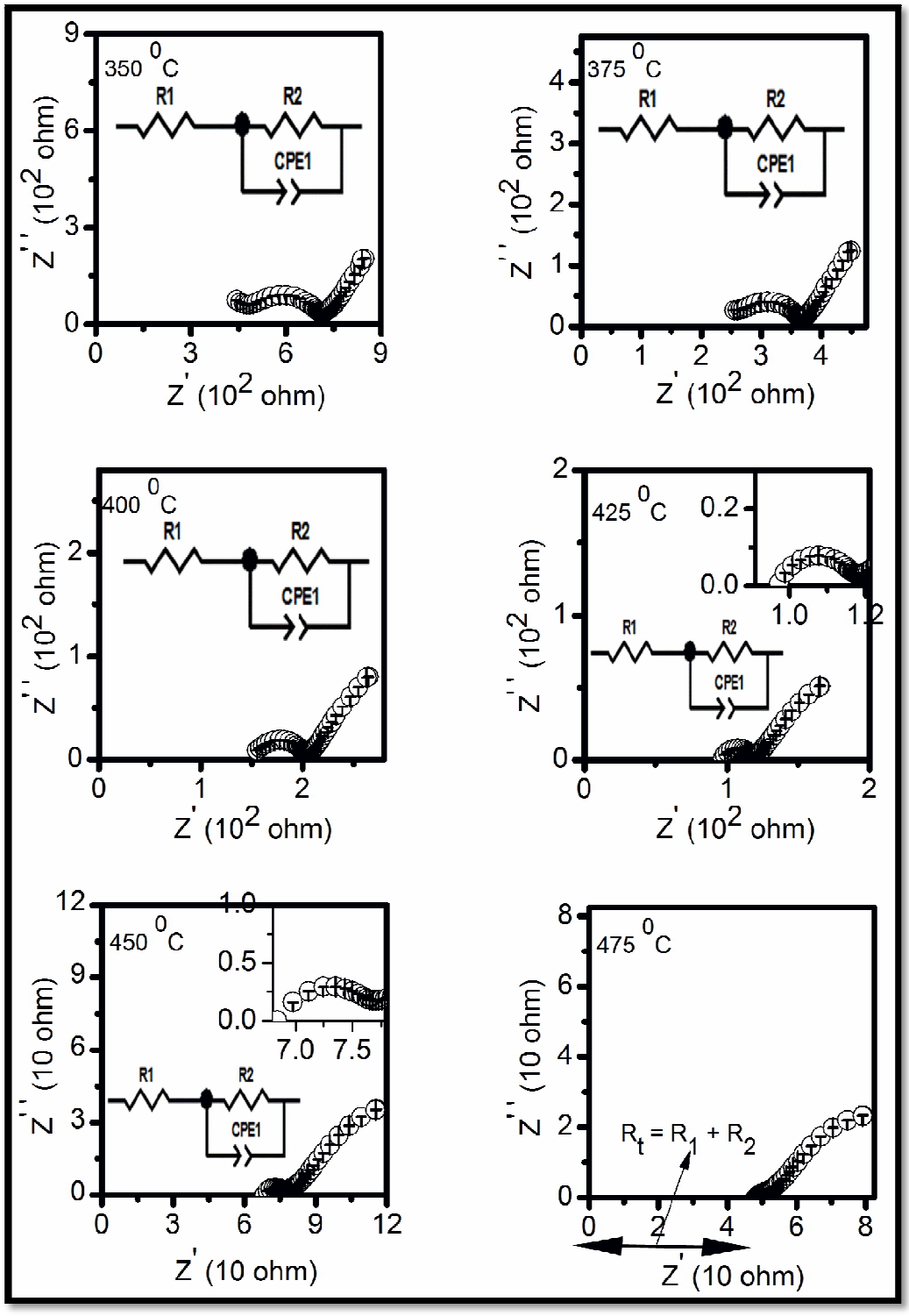

Fig. 7.6 Complex plane impedance plots of the composition CCO5 at different temperatures

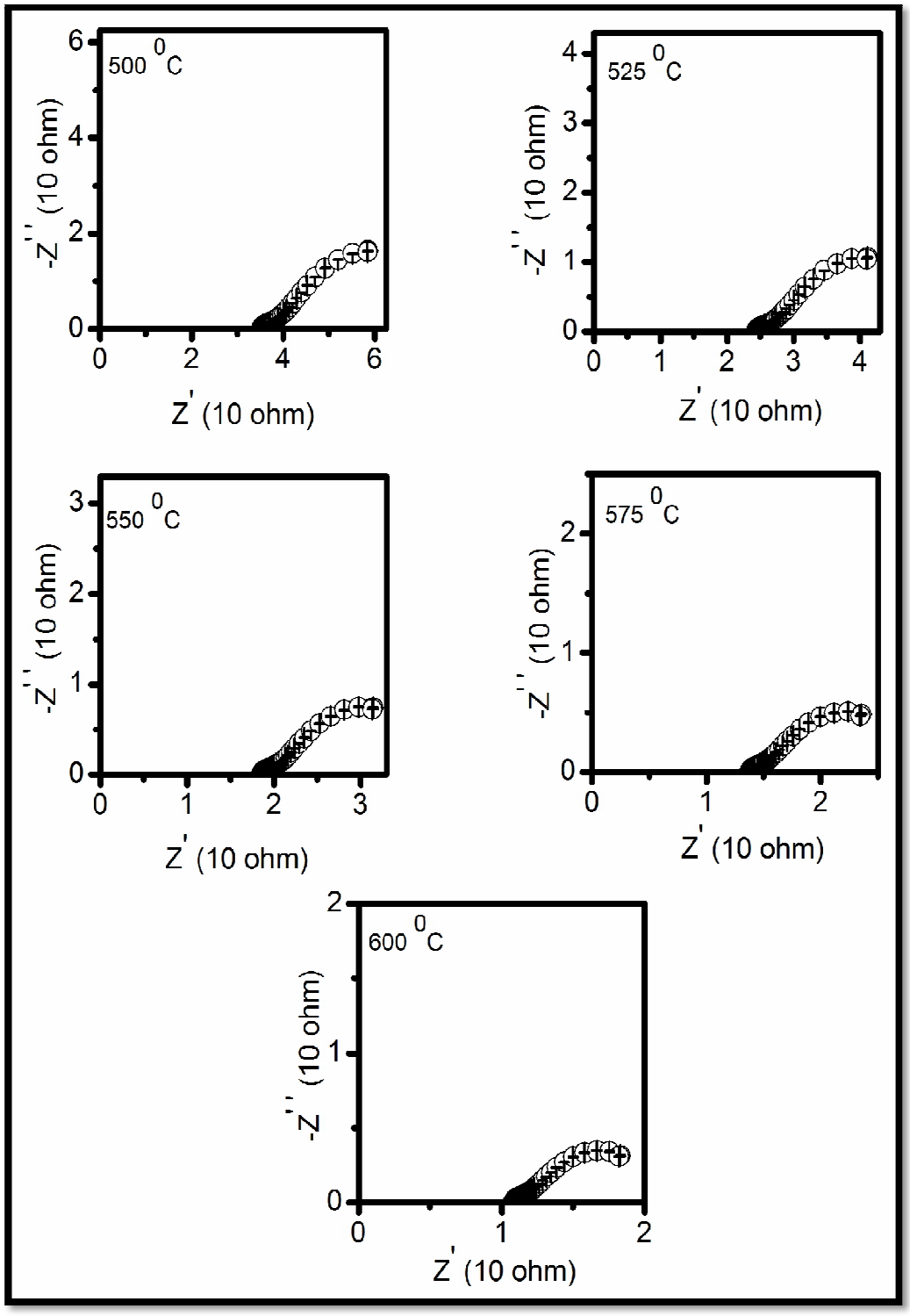

Fig. 7.6 Complex plane impedance plots of the composition CCO5 at different temperatures

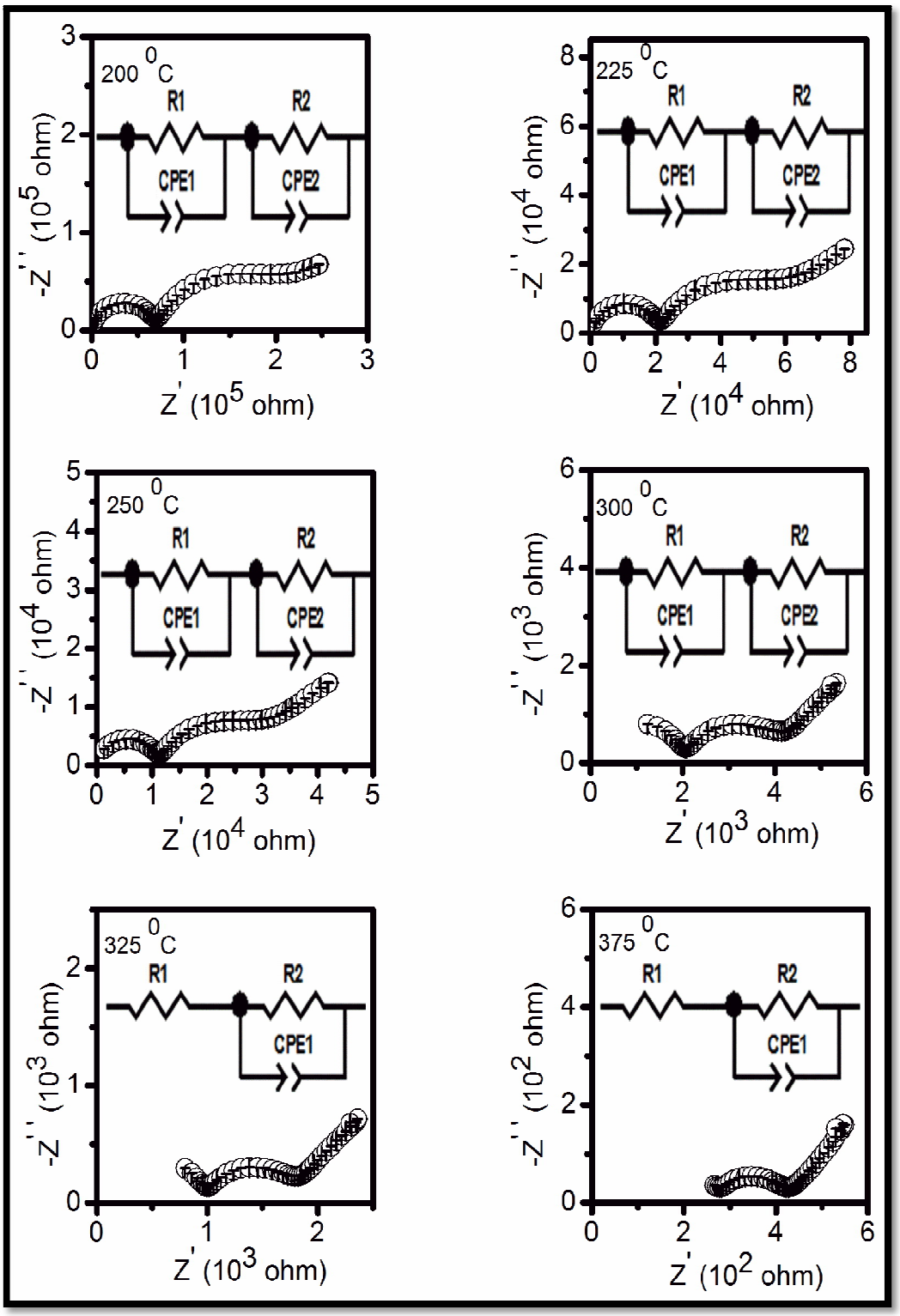

Fig. 7.7 Complex plane impedance plots of the composition CC5S1 at different temperatures

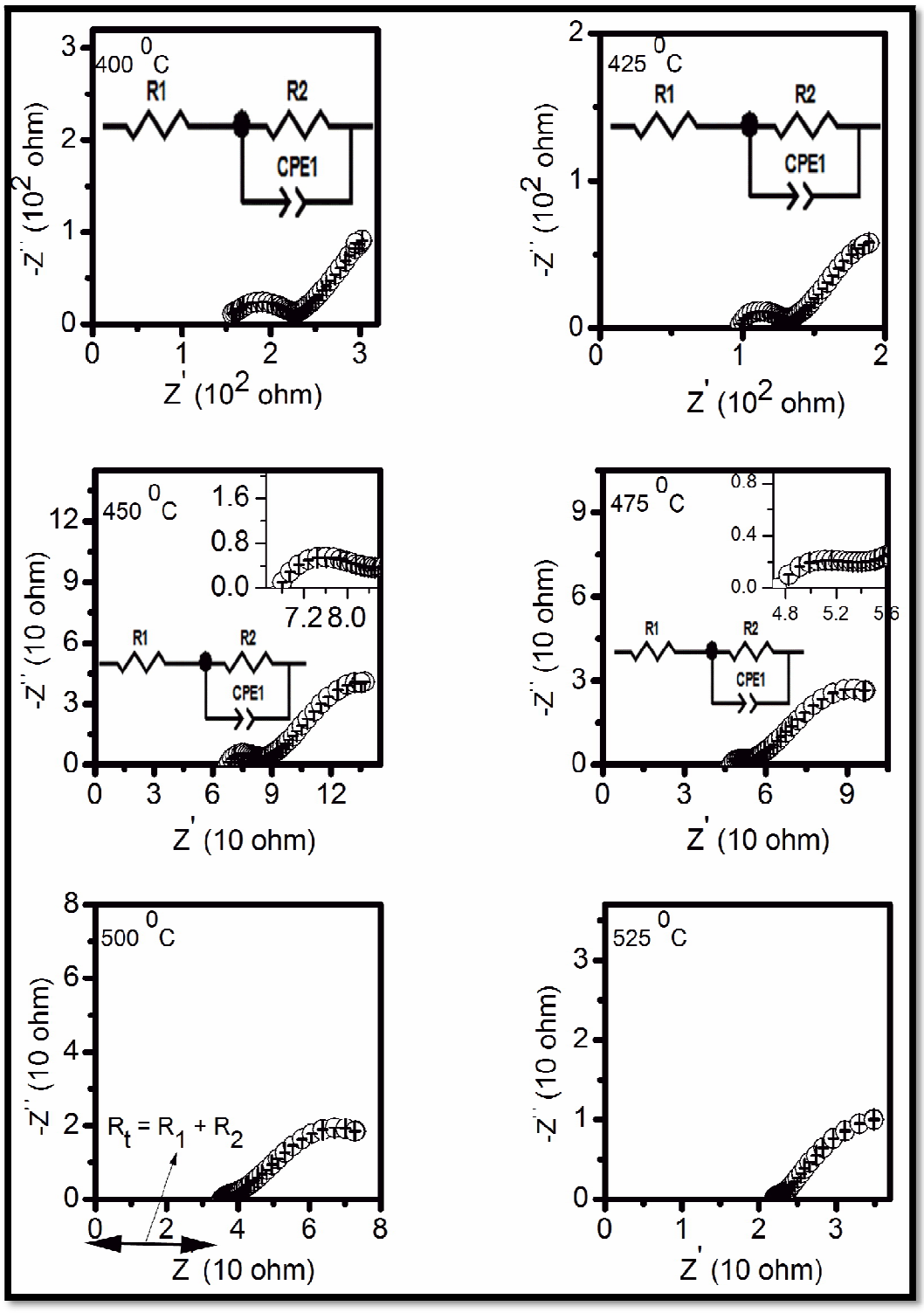

Fig. 7.7 Complex plane impedance plots of the composition CC5S1 at different temperatures

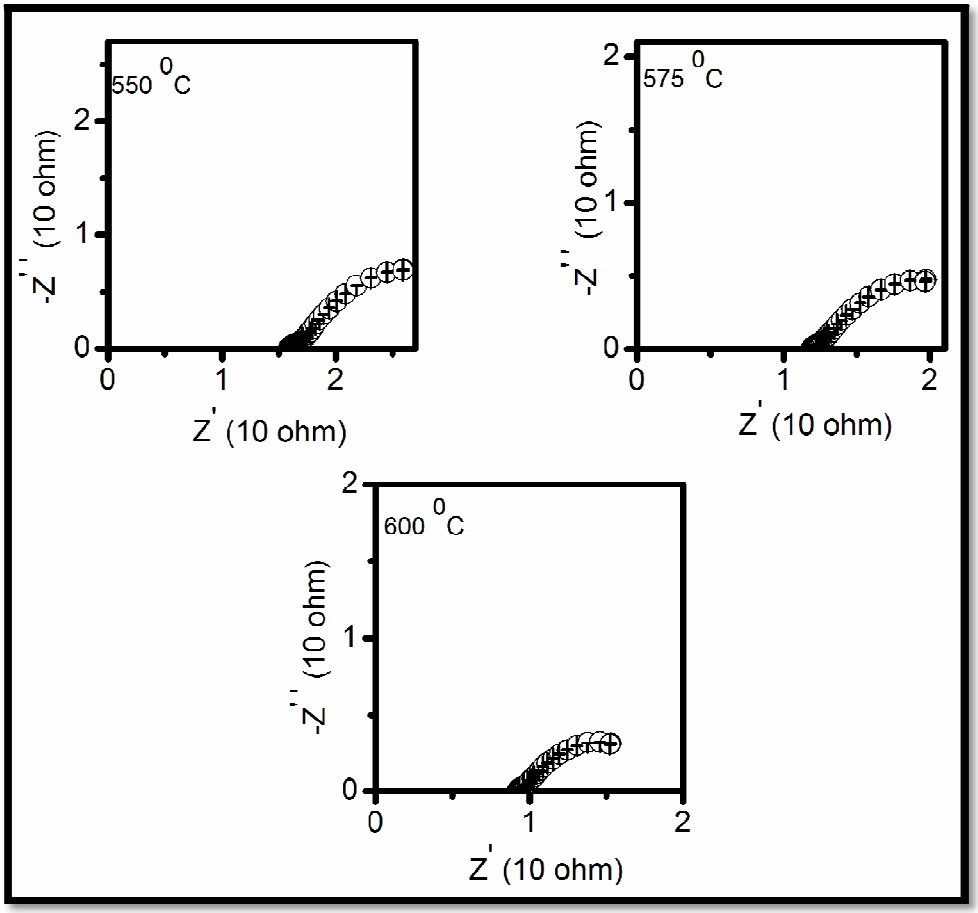

Fig. 7.7 Complex plane impedance plots of the composition CC5S1 at different temperatures

For the composition, CC5S2, the arcs ascribed to the contribution of the grains and the grain boundaries disappear above 275 and 450 °C respectively. In the case of CC5S3, the arc due to the grains and the grain boundaries disappear above 300 and 450 °C respectively. At higher temperatures, only the arc due to contribution of the electrode/specimen interface has been observed for all the compositions.

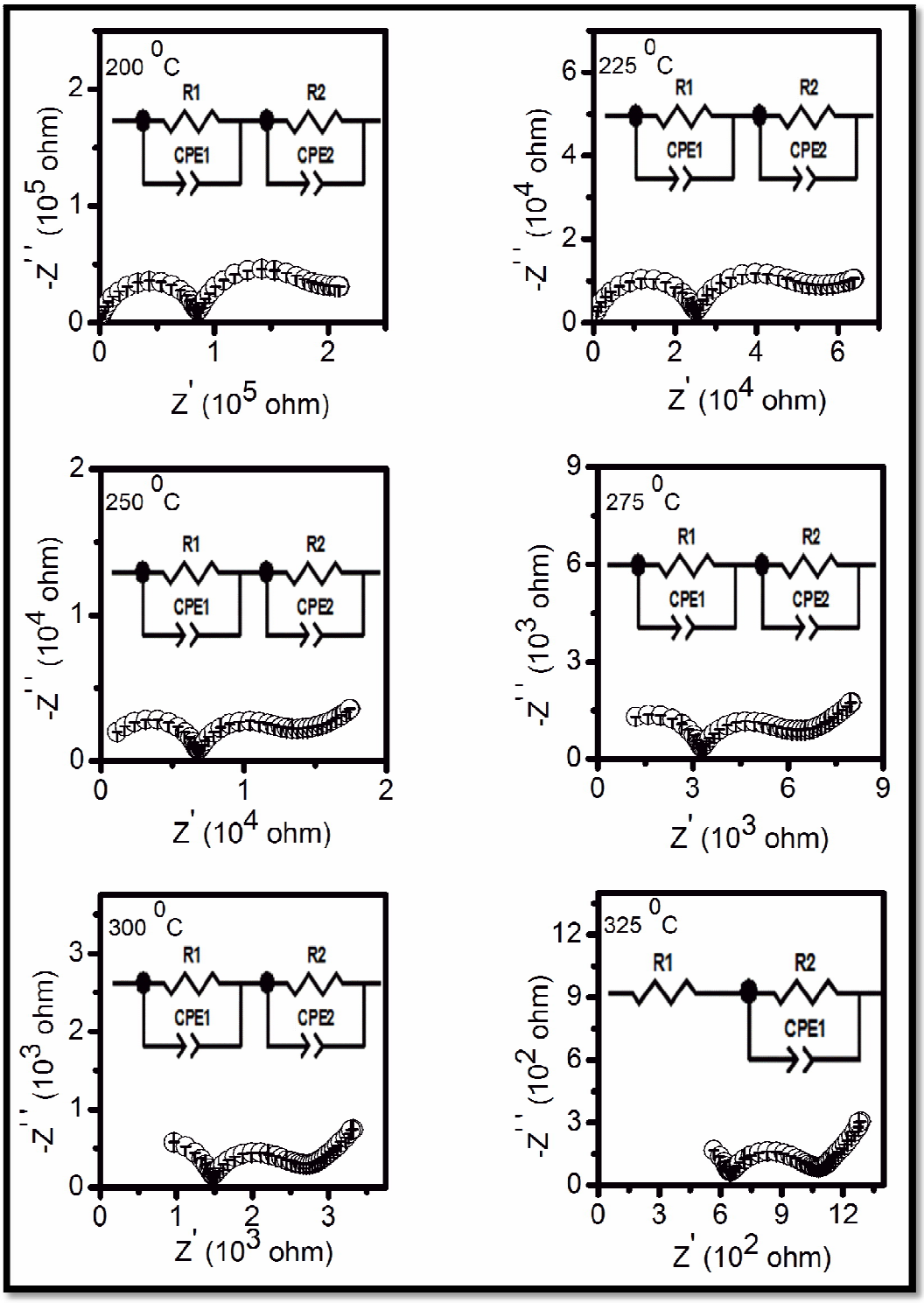

Fig. 7.8 Complex plane impedance plots of the composition CC5S2 at different temperatures

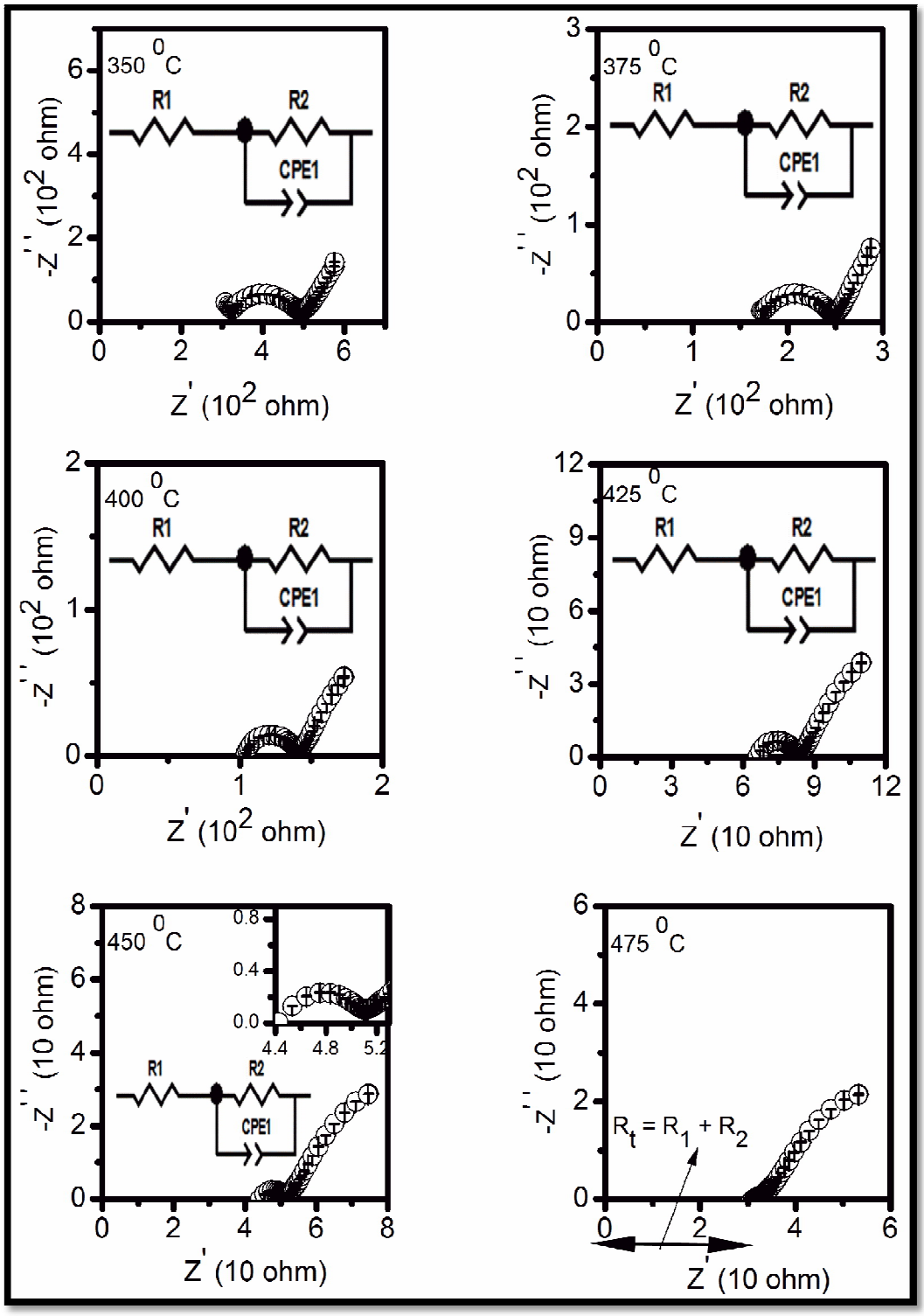

Fig. 7.8 Complex plane impedance plots of the composition CC5S2 at different temperatures

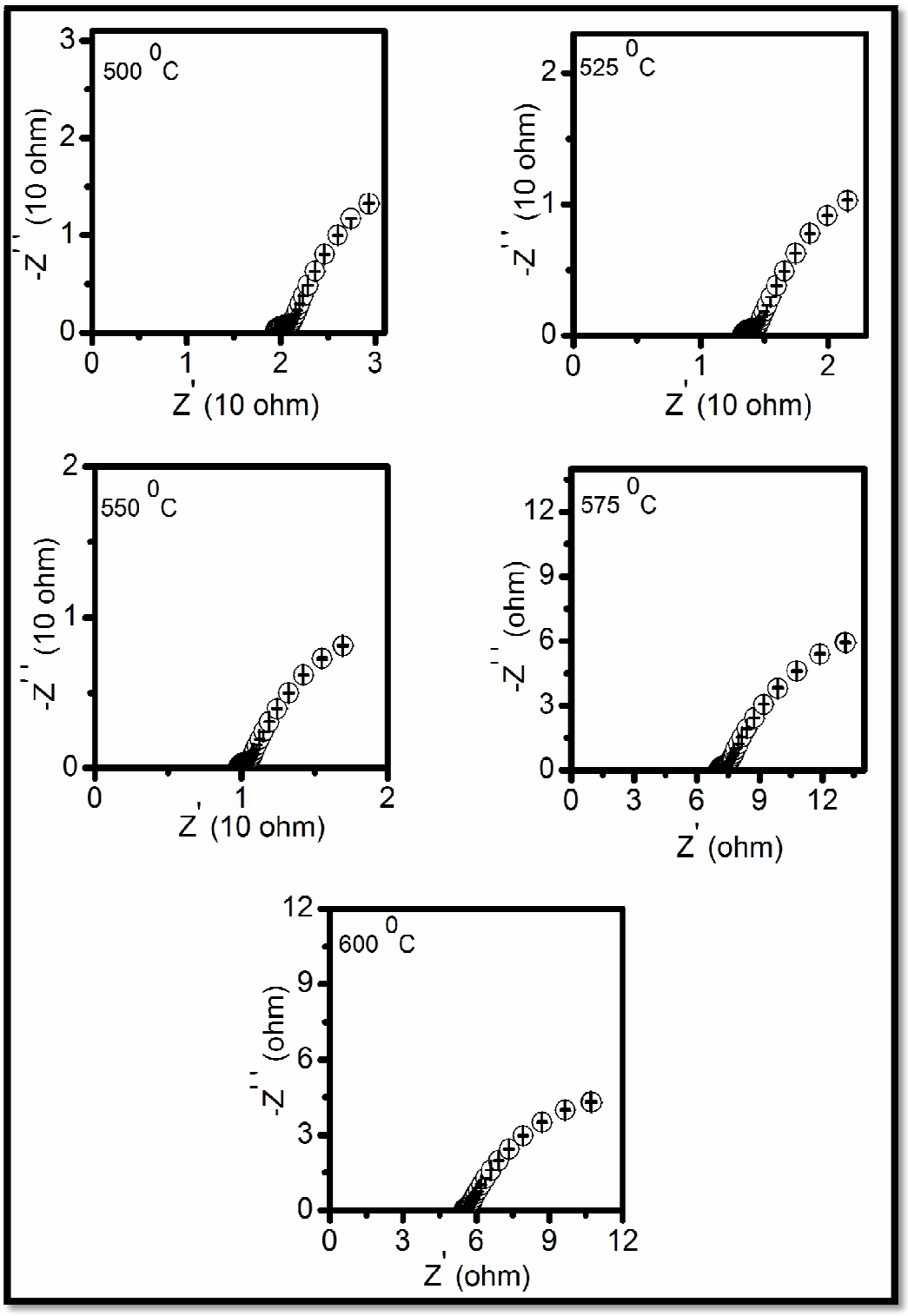

Fig. 7.8 Complex plane impedance plots of the composition CC5S2 at different temperatures

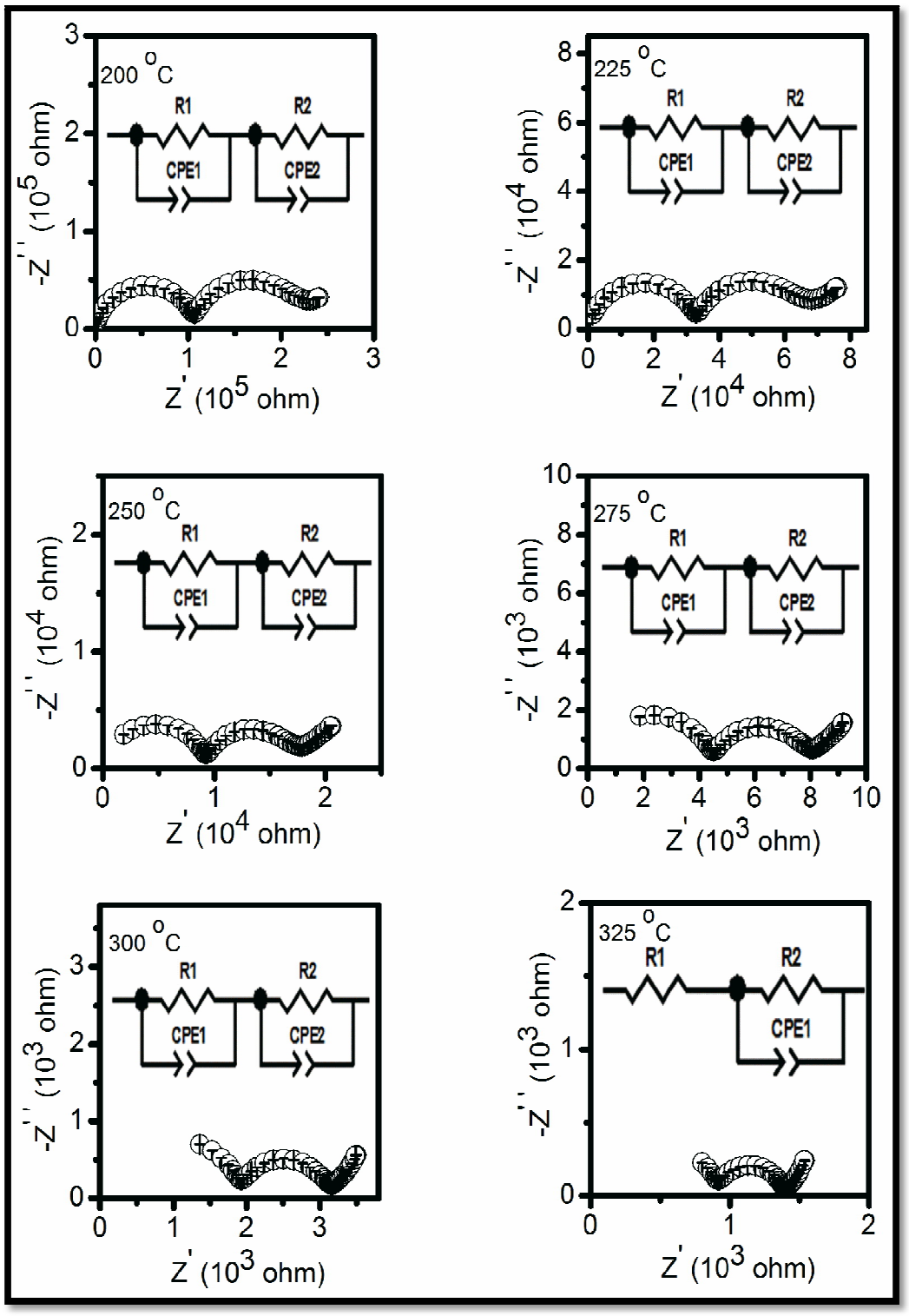

Fig. 7.9 Complex plane impedance plots of the composition CC5S3 at different temperatures

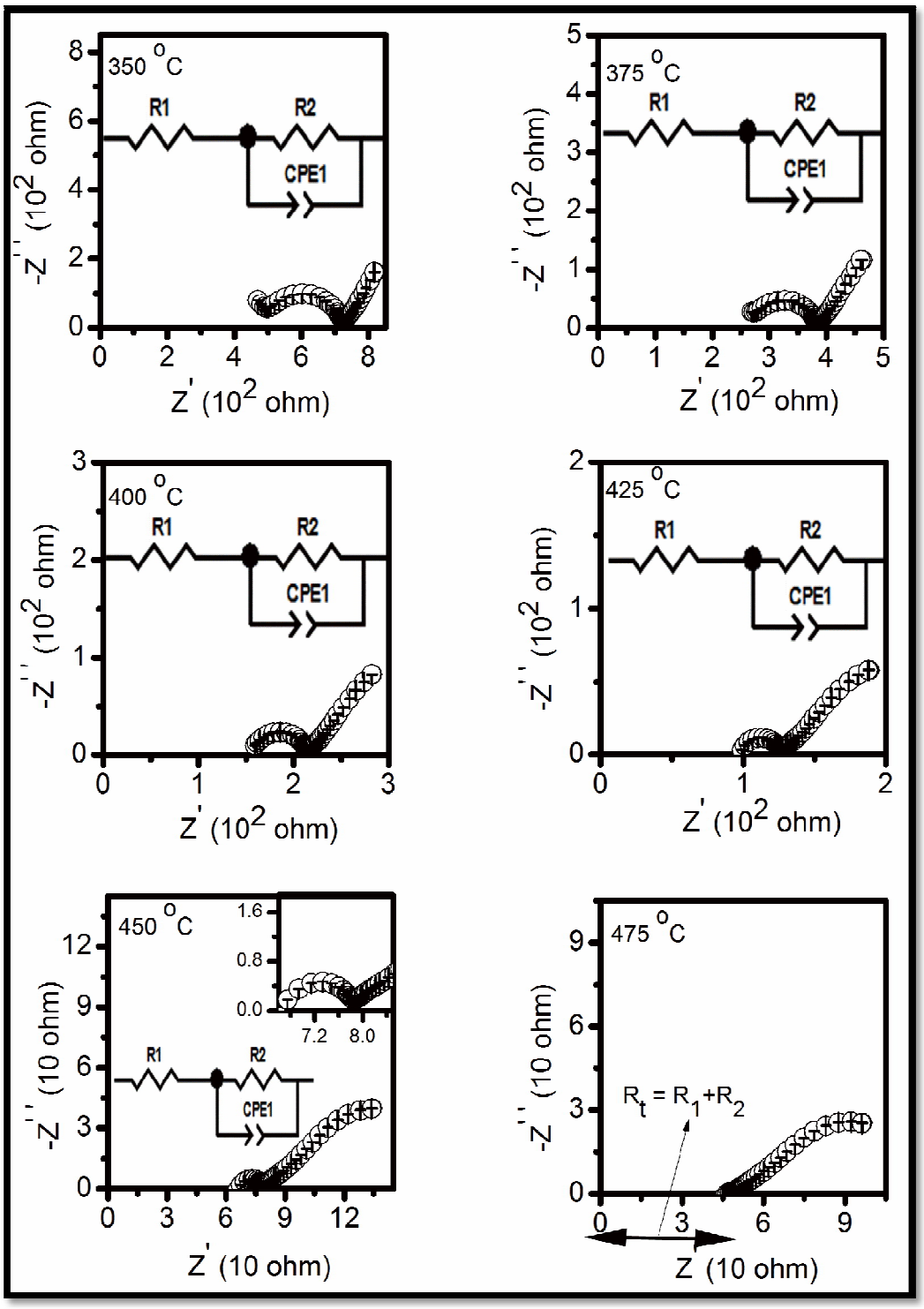

Fig. 7.9 Complex plane impedance plots of the composition CC5S3 at different temperatures

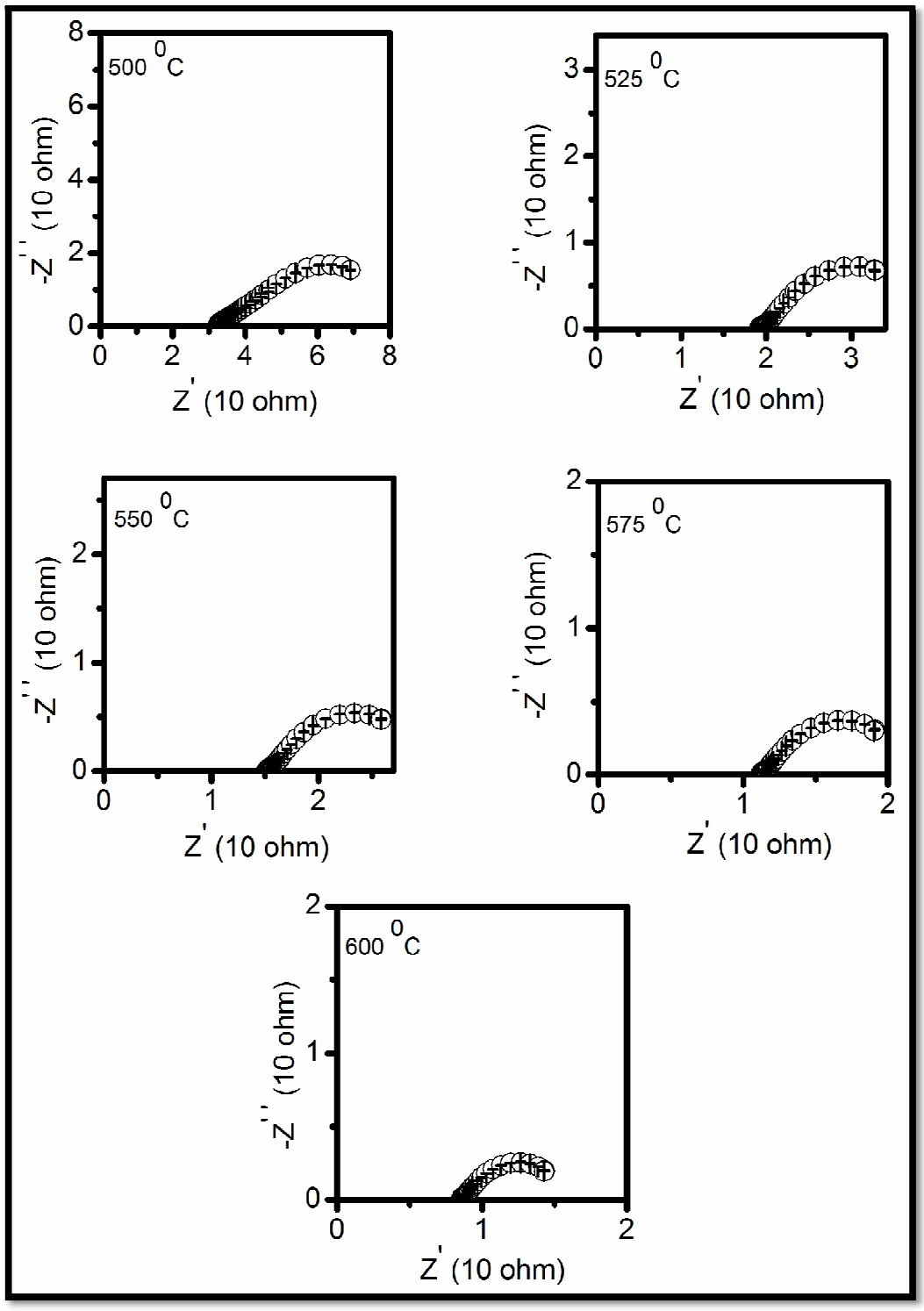

Fig. 7.9 Complex plane impedance plots of the composition CC5S3 at different temperatures

Arrhenius plots for the conductivity of the grains (bulk), grain boundaries and total conductivity of all the compositions are shown in Fig. 7.10. An important feature of ceria is its tolerance to doping due to its relatively open structure. Addition of divalent cations in ceria produces oxygen vacancies responsible for ionic conduction [Trejo et al. (2007); Wang et al. (1981)] as given below in the Eqs. (7.1) and (7.2).

$$SrO \xrightarrow{CeO_2} Sr''_{Ce} + O_O + V_O^{\bullet\bullet} \tag{7.1}$$

$$CaO \xrightarrow{CeO_2} Ca''_{Ce} + O_O + V_O^{\bullet\bullet} \tag{7.2}$$

It is seen from Fig. 7.10 that the bulk conductivity, σ_g, is the highest for the sample, $Ce_{0.93}Ca_{0.05}Sr_{0.02}O_{1.93}$ and starts decreasing for x (Sr) > 0.02. Value of σ_g for the sample, $Ce_{0.93}Ca_{0.05}Sr_{0.02}O_{1.93}$ is 1.39×10^{-4} S/cm at 325 ^oC which is much higher than the value 6.0×10^{-6} S/cm reported by Junior et al. [Junior et al. (2012)] for the sample $Ce_{0.90}Ca_{0.05}Sr_{0.05}O_{1.90}$ at 320 ^oC. Activation energy of conduction, E_g, determined by fitting the data points to Arrhenius equation is given in Table. 7.2.

It is noted from Fig. 7.10 that the grain boundaries conductivity is higher for the co-doped samples. This may be due to two factors. One is the scavenging effect of Sr and second is the average grain size. Value of the scavenging factor or blocking factor, $\propto_{gb}$ is 0.37 for the sample $Ce_{0.95}Ca_{0.05}O_{1.95}$ which is maximum and 0.11 for $Ce_{0.93}Ca_{0.05}Sr_{0.02}O_{1.93}$ being minimum of all the samples. This may be due to scavenging effect of Sr^{2+} ions to remove siliceous impurities. It has been reported by Gerhardt et al. (1986) that grain boundary effect depends on the dopant concentration and dopant size. The grain boundary resistivity decreases sharply with increasing concentration and size of the dopant [Gerhardt et al. (1986)]. Concentration and nature of the dopant control how much Si goes into solid solution and how much is segregated. Removal of silica decreases the resistivity of the grain boundaries leading to decrease in the total resistivity. In the present investigation an optimum value of Sr concentration for the scavenging effect is 2 mol%. It can be observed from Fig. 7.10 that the conductivity of the grain boundaries for co-doped samples increases with decreasing average grain size. Small grain size samples exhibit much higher grain boundaries conductivity.

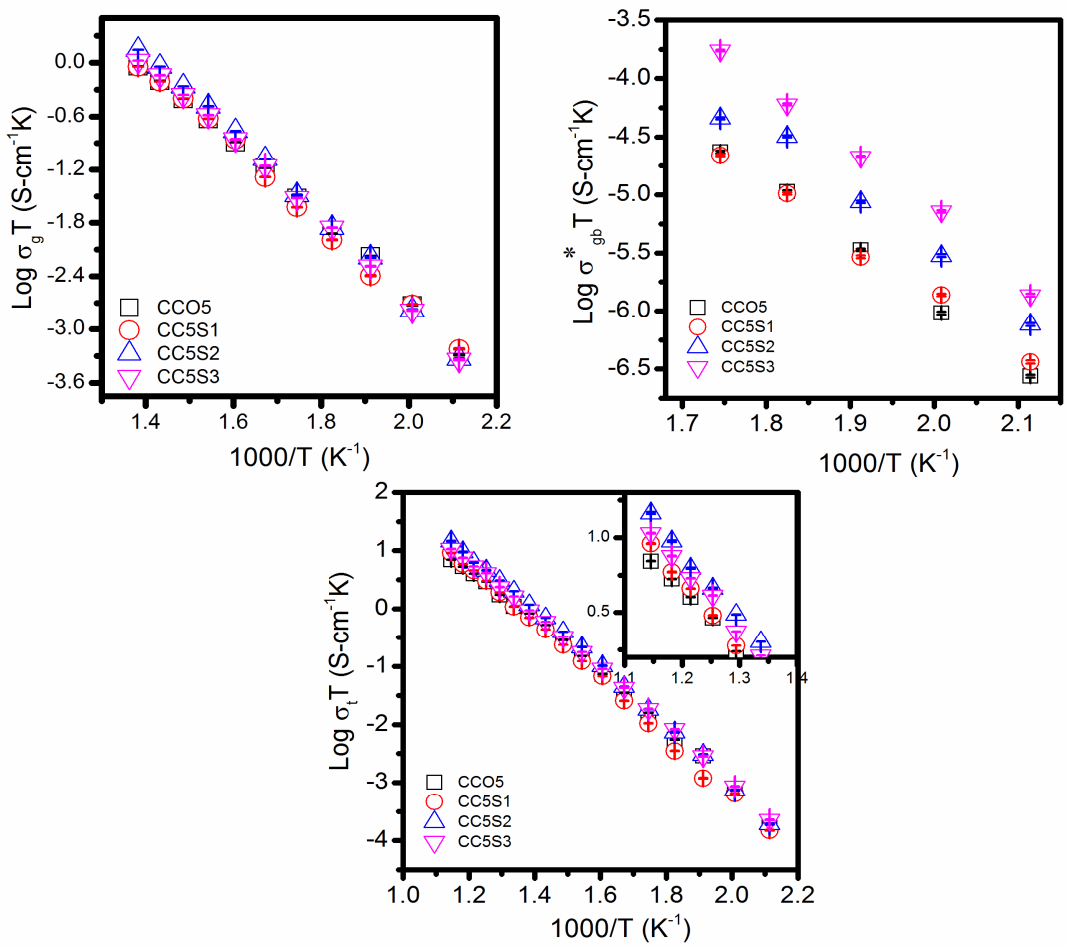

Fig. 7.10 Arrhenius plots for the grain, grain boundaries and total ionic conductivity of all the composition

This is because of the large area of the grain boundaries for which the finite amount of impurity contained in these samples is not sufficient to form a continuous and uniform glassy phase layer along the grain boundaries. This leaves the remaining area of the boundaries for clean grain to grain contact. Therefore, the transport of O^{2-} ions becomes faster across the clean grain boundaries.

Plots of Log $\sigma_t T$ vs 1000/T are linear with a single slope. The activation energy of total conductivity and pre-exponential factor (σ_0) determined from the slope and intercept respectively of these plots are given in Table. 7.2. Values of σ_t at 600 °C for different compositions are given in Table. 7.3. Value of σ_t increases with increasing Sr content up to 2 mol%. It is also observed from the Tables. 7.2 & 7.3 that the composition showing the maximum conductivity does not has the minimum

activation energy. It is also noted that the minimum activation energy is not observed in the sample having the maximum pre-exponential factor. It is concluded that pre-exponential factor depends on the dopant concentration i.e. the maximum of electrical conductivity and minimum activation energy are not always associated with the same dopant concentration [Inba et al. (1996)]. The composition, CC5S2 has the maximum σ_0 and the maximum conductivity.

Table. 7.2 Activation energy for conductivity of grains (E_g), grain boundaries (E_{gb}), total (E_t) and pre-exponential factor (σ_0)

S. No.	x	Sample code	E_g (eV) (200-450 °C)	E_{gb} (eV) (200-450 °C)	E_t (eV) (200-600 °C)	σ_0
1.	0.0	CCO5	0.88	1.06	0.93	2.09×10^{6}
2.	0.01	CC5S1	0.89	0.97	0.99	5.01×10^{6}
3.	0.02	CC5S2	0.94	1.10	0.97	8.13×10^{6}
4.	0.03	CC5S3	0.92	1.11	0.95	3.71×10^{6}

Table. 7.3 Total conductivity (σ_t) and configurational entropy (S) of all the compositions

S. No.	x	Sample code	σ_t at 600 °C (S/cm)	S (J/mol K)
1.	0.0	CCO5	7.98×10^{-3}	1.65
2.	0.01	CC5S1	1.04×10^{-2}	2.11
3.	0.02	CC5S2	1.66×10^{-2}	2.45
4.	0.03	CC5S3	1.22×10^{-2}	2.75

In the present study, an addition of Ca and Sr to ceria leads to some opposite competiting effects. First the concentration of oxygen vacancies increases with

increasing the Sr content. Second, the ordering of oxygen vacancies is suppressed due to co-doping causing an increase in the configurational entropy (Table. 7.3) [Yamamura et al. (2000)]. This decreases the activation energy for migration of O^{2-} ion leading to an increase in the conductivity. Third, scavenging effect of Sr^{2+} increases the conductivity of the grain boundaries as well as the total conductivity. Pre-exponential factor also increases due to co-doping of Sr. This also causes an increase in the total conductivity. Fourth, the ionic size mismatch between Sr^{2+} (1.26 Á) and Ce^{4+} (0.97 Á) is larger than that between Ca^{2+} (1.12 Á) and Ce^{4+} (0.97 Á). The elastic strain therefore increases with increasing x (Sr). This decreases the conductivity because of an increase in the activation energy for diffusion of O^{2-} ion [Yamamura et al. (2000)]. Concentration of oxygen vacancies also increases with increasing x. At the same time the probability of formation of the associated defect pairs ($Ca''_{Ce} - V_O^{\bullet\bullet}$ or $Sr''_{Ce} - V_O^{\bullet\bullet}$) also increases with increasing x. Due to complex interplay of these opposite competiting effects, conductivity increases up to x = 0.02, and decreases thereafter. The composition, CC5S2 shows the highest conductivity among all the compositions studied. Its conductivity at 600 °C (1.66×10^{-2} S/cm) is higher than the reported values of conductivity for the compositions $Ce_{0.80}Sm_{0.20}O_{1.90}$ (1.20×10^{-2} S/cm) [Balazas et al. (1995)], and $Ce_{0.80}Gd_{0.20}O_{1.90}$ (1.29×10^{-2} S/cm) [Fu et al. (2010)] at 600 °C. Use of this material as a solid electrolyte for IT-SOFC is expected to reduce the cost significantly.

7.1.3 Conclusion

- Samples in the system, $Ce_{0.95-x}Ca_{0.05}Sr_xO_{1.95-x}$ (x = 0.00, 0.01, 0.02 and 0.03), have been prepared successfully by citrate-nitrate route.
- Single phase solid solution has formed in all the compositions.
- Density of all the samples is more than 97% of the theoretical value.
- Bulk conductivity as well as the total conductivity of co-doped samples increases with an increase in Sr concentration up to 2 mol% and decreases with further addition of Sr.
- Composition with x = 0.02 exhibits the maximum ionic conductivity. This is higher than the maximum values reported in the system, SDC and GDC.

- This may make this material suitable as a solid electrolyte for IT-SOFCs application.

7.2 Nanocomposites of Ca and Sr Co-Doped Ceria (CC5S2)

7.2.1 Introduction

Doped ceria, however, exhibits mixed electronic and ionic conduction in reducing atmosphere. This leads to a loss of open circuit voltage (OCV) and a drop in the power output of the cell. It may also cause lattice expansion of the electrolyte because ionic radius of Ce^{4+} and Ce^{3+} with 8 co-ordinations is 0.97 Å and 1.143 Å [Shannon (1976)] respectively. This results in mechanical instability of the cell. Electronic conduction occurs due to hopping of electrons among Ce^{4+} and Ce^{3+} ions.

In the recent years, a novel strategy of ceria/salt based nanocomposite electrolytes has been developed for low temperature SOFCs (LT-SOFCs). This reduces the electronic conduction [Zhu (2003)]. These composites consist of two phases: one is the crystalline ceria based phase and the second is an amorphous salt phase. A typical ceria/salt composite is the ceria/carbonates composite [Zhu et al. (2006)]. The composite electrolytes show a high ionic conductivity (> 0.1 S/cm) above the melting point of the carbonate (400-500 °C). A single cell based on this material has been reported to have a high performance in the intermediate temperature range, e.g. 1700 mW-cm^{-1} at 650 °C [Xia et al. (2009); Xia et al. (2010)].

In the above reported results in the section 1 for Ca^{3+} and Sr^{2+} co-doped ceria, it is observed that the composition $Ce_{0.93}Ca_{0.05}Sr_{0.02}O_{1.93}$ (CC5S2) shows the highest conductivity (1.66×10^{-2} S/cm at 600 °C) of all the compositions. In this section, nanocomposite electrolytes based on CC5S2/$(Li\text{-}Na)_2CO_3$ (CC5S2/LNCO) have been prepared and characterized.

7.2.2 Results and Discussion

(a) Thermal analysis

DTA plots of all the composite samples are shown in Fig. 7.11. Two endothermic peaks have been observed in the DTA plot of all the composites. One is observed around 100 °C which corresponds to evaporation of adsorbed moisture in the sample.

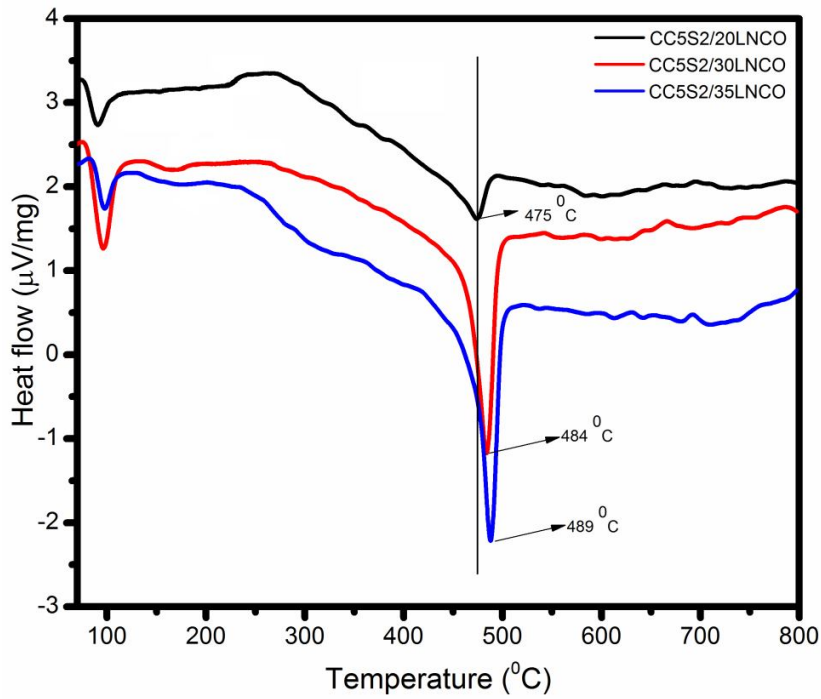

Fig. 7.11 DTA plots of all the samples in the system CC5S2/LNCO

Second endothermic peak is observed at 475, 484 and 489 °C for the compositions, CC5S2/20LNCO, CC5S2/30LNCO and CC5S2/35LNCO respectively. This is ascribed to the melting of eutectic carbonate mixture. There is no peak beyond 500 °C. Therefore, the composite samples were calcined at 600 °C for 2 hrs.

(b) Crystal structure and phases

Powder X-ray diffraction (XRD) patterns of all the milled (before calcination), calcined and sintered samples are recorded. Fig. 7.12 shows the XRD patterns of all the sintered composite samples along with CC5S2. All the peaks have been indexed using JCPDS file no. 43-1002 of ceria having fluorite structure. All the samples have been found to be single phase solid solution i.e. there is no peak of carbonate phase. This confirms that carbonates exist as an amorphous phase in the milled and calcined samples as well in the sintered samples. XRD patterns of the uncalcined samples are the same as that of the calcined and sintered samples except that the peaks become sharp after sintering. Diffraction peaks of the uncalcined samples are very broad.

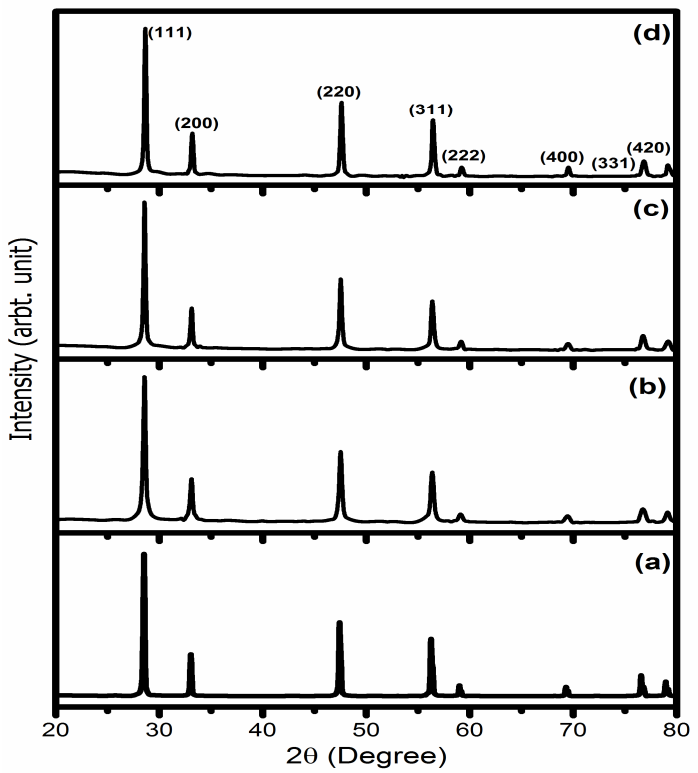

Fig. 7.12 XRD patterns of all the sintered samples of compositions (a) CC5S2 (b) CC5S2 /20 LNCO (c) CC5S2 /30 LNCO and (d) CC5S2 /35LNCO

Average crystallite size of the milled composite powders (uncalcined) has been found to be in the range 22-30 nm using Scherrer's formula. These nanosized particles will produce large interfacial region due to large surface area and create highways for the conduction of ions. Compositions, CC5S2/20LNCO, CC5S2/30LNCO and CC5S2/35LNCO have density 88%, 87% and 85% of the theoretical value after sintering at 700 °C. The low density is due to sintering at low temperature. These composites, however, can still be used as electrolytes for SOFCs because carbonates melt at working temperature and serve as seal to avoid crossover of the gases and also increase the mechanical strength [Di et al. (2010)].

(b) Microstructure

Micrographs of all the sintered samples are given in Fig. 7.13 (a)-(d). Micrograph of CC5S2 (sintered at 1350 °C) is very dense with an average grain size of 2 μm. Composites show porous microstructure due to low sintering temperature. The grains

are fully covered by an amorphous carbonate phase. Average grain size of the sintered composite samples is about 100-120 nm because the grain growth is inhibited by the amorphous molten carbonate phase. Due to this morphology of the composites, percolation of molten carbonate is obvious causing a large interface region between the two phases. EDS of the composition, CC5S2/35LNCO at two different points is shown in Fig. 7.14. All the constituent elements are present in the expected stoichiometry except Li.

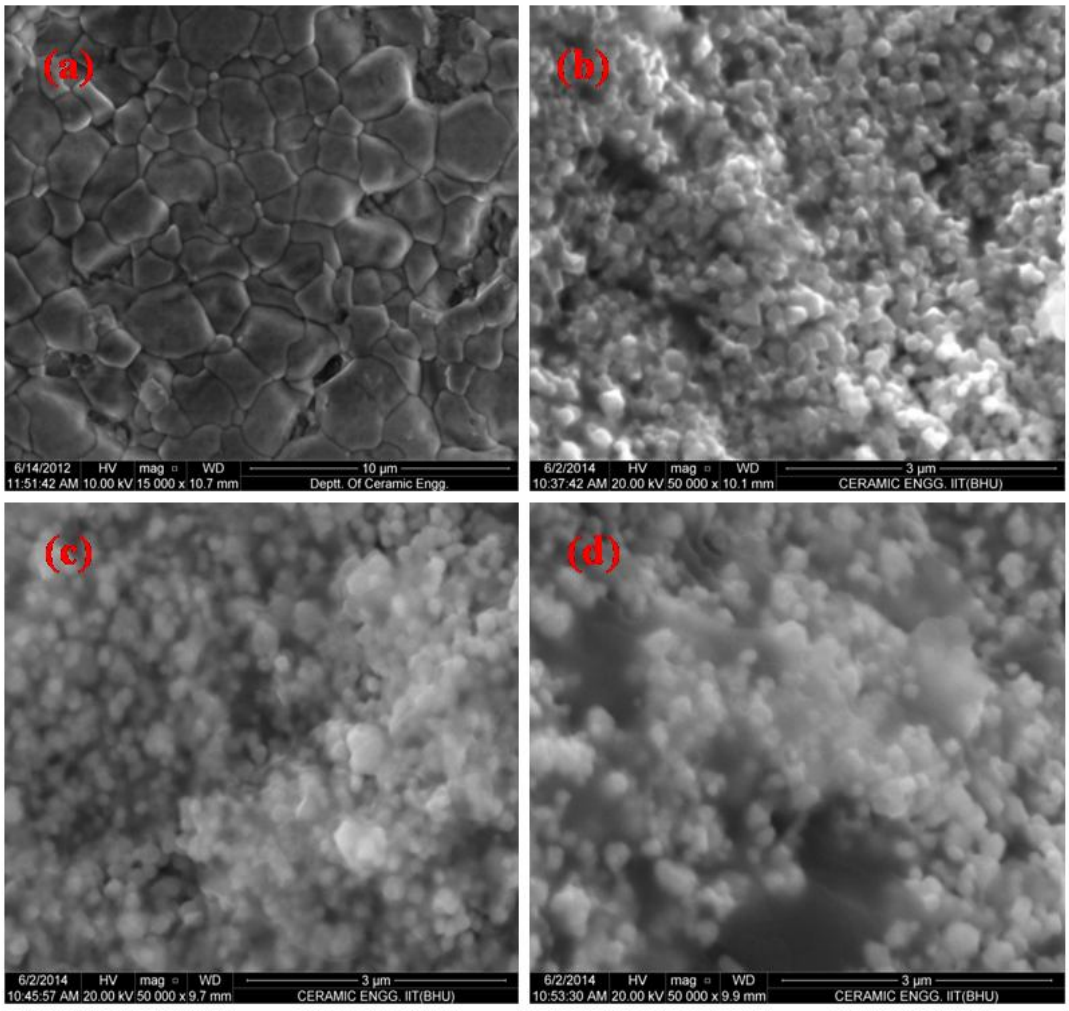

Fig. 7.13 SEM micrographs of all the sintered samples (a) CC5S2: thermally etched (b) CC5S2 /20 LNCO: fractured sample (c) CC5S2/30 LNCO: fractured sample and (d) CC5S2/35 LNCO: fractured sample

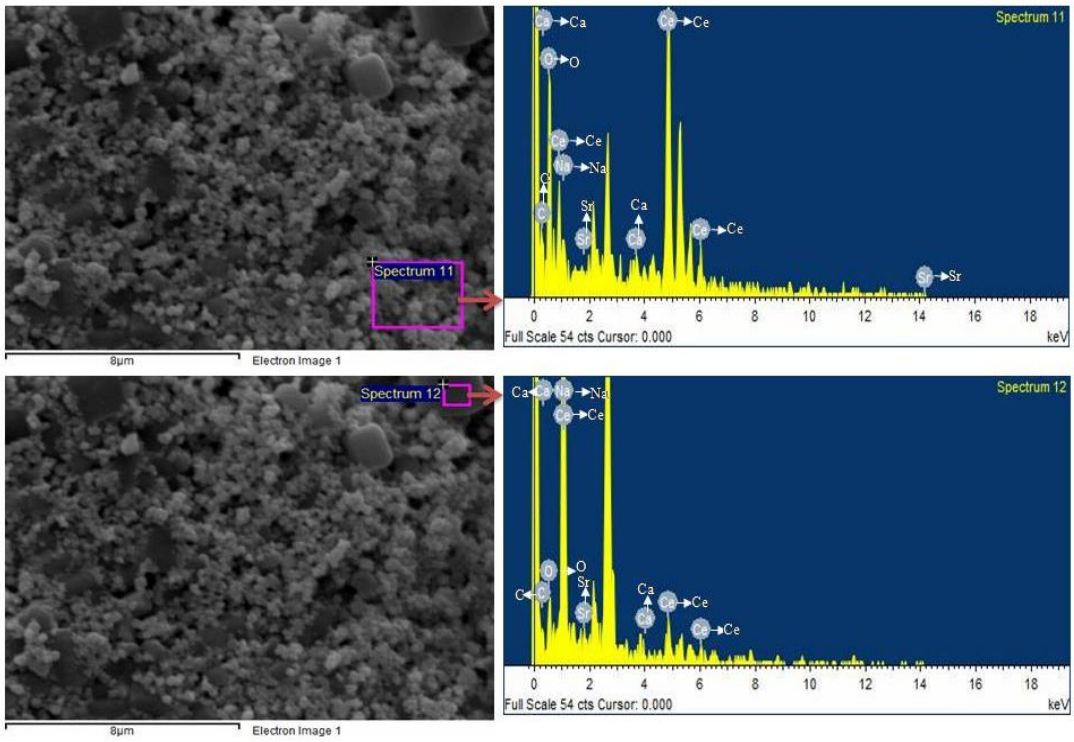

Fig. 7.14 EDS of the composition CC5S2/35LNCO at two different points

It is noted from Fig. 7.14 that the light grey region (spectrum 11) represents the crystalline ceria phase containing higher concentration of heavy ions. The dark region (spectrum 12) represents the amorphous carbonate phase having less percentage of heavy ions.

(d) Thermal expansion

Plots of thermal expansion of all the composites are shown in Fig. 7.15. These curves show a non-linear behavior. Two inflection points have been observed in all the samples. First is at 325 °C, 400 °C and 445 °C for the compositions, CC5S2/20LNCO, CC5S2/30LNCO and CC5S2/35LNCO respectively. This corresponds to the softening of the carbonate phase. Around 500 ºC, the remaining carbonates melt and fill in the interspaces forming a continuous path. This causes again a linear expansion above 500 °C. This gives second inflection point. Values of CTE of all the composites are given in Table. 7.4.

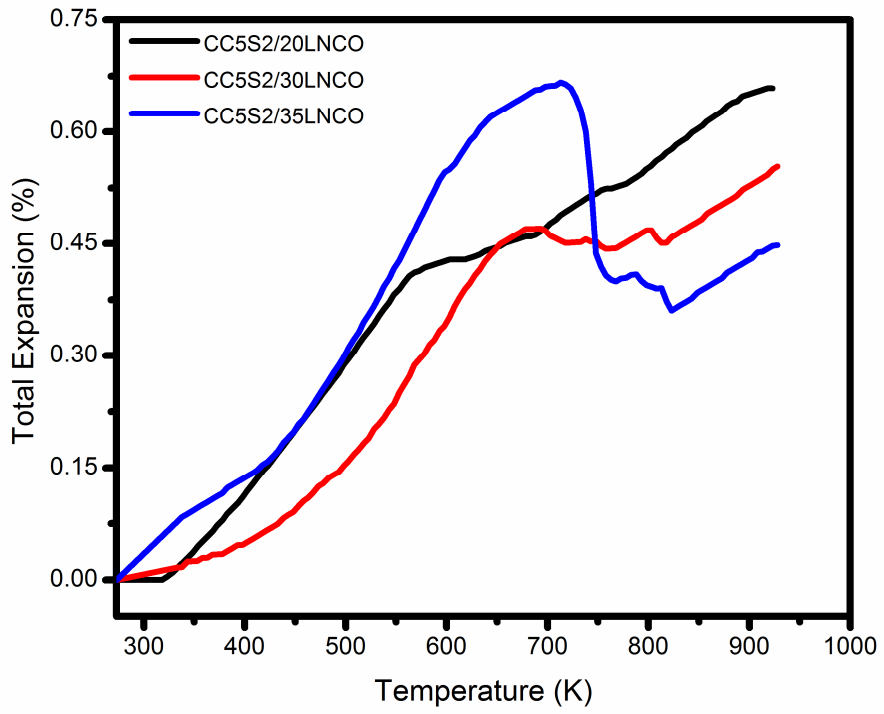

Fig. 7.15 Thermal expansion curves for CC5S2/LNCO composites

Table. 7.4 Coefficient of thermal expansion of all the samples

S. No.	Compositions	CTE (K^{-1})
1.	CC5S2/20LNCO	13.0×10^{-6}
2.	CC5S2/30LNCO	11.0×10^{-6}
3.	CC5S2/35LNCO	25.3×10^{-6}

(e) Electrical conductivity

Complex plane impedance plots of all the composites at different temperatures are shown in Figs. 7.16-7.18. For the compositions, CC5S2/20LNCO and CC5S2/30LNCO, a high frequency arc along with a tail at lower frequency has been observed. The high frequency arc is ascribed to the contribution of the grains and a tail is ascribed to contribution of the electrode/electrolyte interface polarization to the total resistance. It is noted from these impedance plots that a distinct grain boundaries arc is absent. This is due to overlapping of the relaxation times of both the grains and grain boundaries polarization processes. This is a distinct feature of the

ceria/carbonate composites in contrast to the single phase doped ceria electrolytes. In the single phase doped or co-doped ceria, distinct grains and grain boundaries arcs have been observed. Relaxation frequency of the polarization processes increases with increase in the temperature. The arcs, therefore, shift towards higher frequency with increasing temperature. The high frequency arc disappears above 300 ℃. Only electrode arc has been observed at high temperatures > 300 ℃. Above 450 ℃, a spike on the low frequency side of the electrode arc has been observed. This is ascribed to a mass transfer process [Di et al. (2010)]. The arc due to the grains has capacitance in the pF (10^{-10}-10^{-12}) range [Hodge et al. (1976)]. It is determined from the relation $2\pi f_{max}RC = 1$ as well as from the fitting of impedance plots using ZView software (value of CPE1).

In the case of composition, CC5S2/35LNCO, a high frequency arc and tail in the low frequency region have been observed. The arc passing through the origin in the high frequency region corresponds to the contribution of the grains to the total resistance. A low frequency tail is ascribed to the contribution of the electrode. The arc of the grains disappears above 325 °C. These plots are fitted to an equivalent circuit containing single R_1-CPE1 element connected in parallel to determine the resistance of the grains (total resistance of the sample). In the present investigation, contribution of the electrode to the total resistance is not considered. The arc of the electrode, therefore, is not fitted. At higher temperatures, an intercept on the real Z' axis on the higher frequency side of the electrode arc has been taken as equal to the total resistance of the sample.

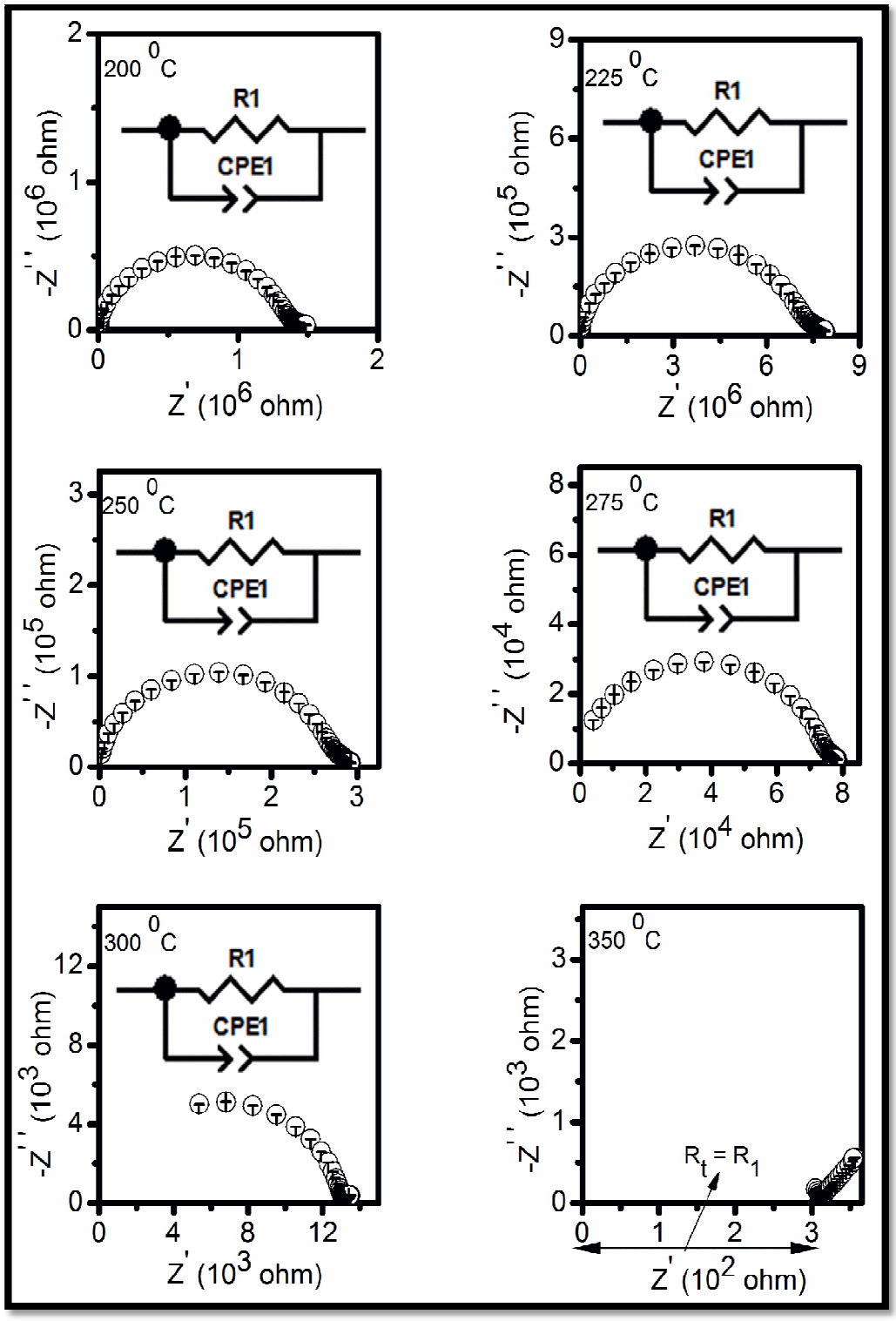

Fig. 7.16 Complex plane impedance plots of the composition CC5S2/20LNCO at different temperatures

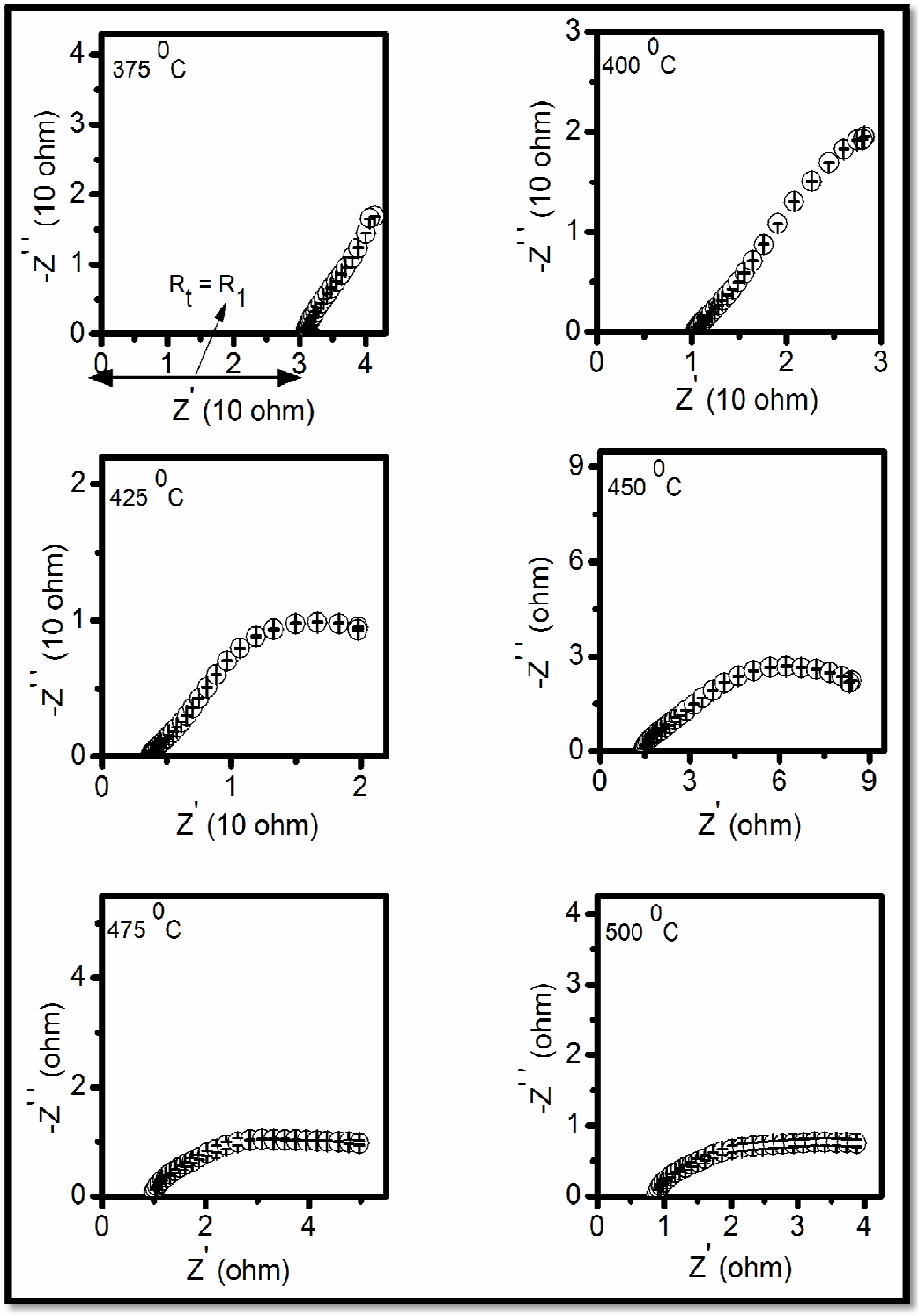

Fig. 7.16 Complex plane impedance plots of the composition CC5S2/20LNCO at different temperatures

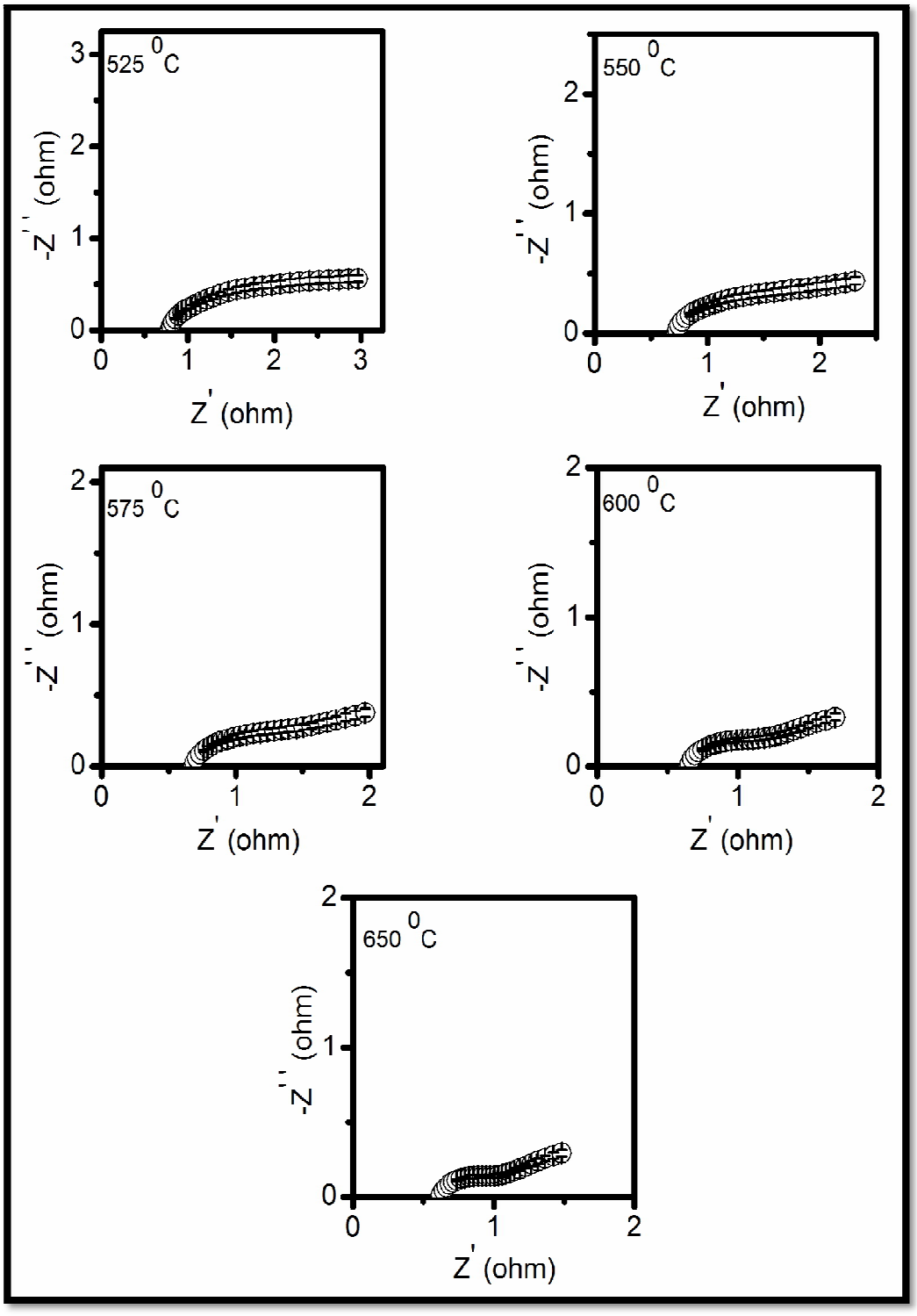

Fig. 7.16 Complex plane impedance plots for the composition CC5S2/20LNCO at different temperatures

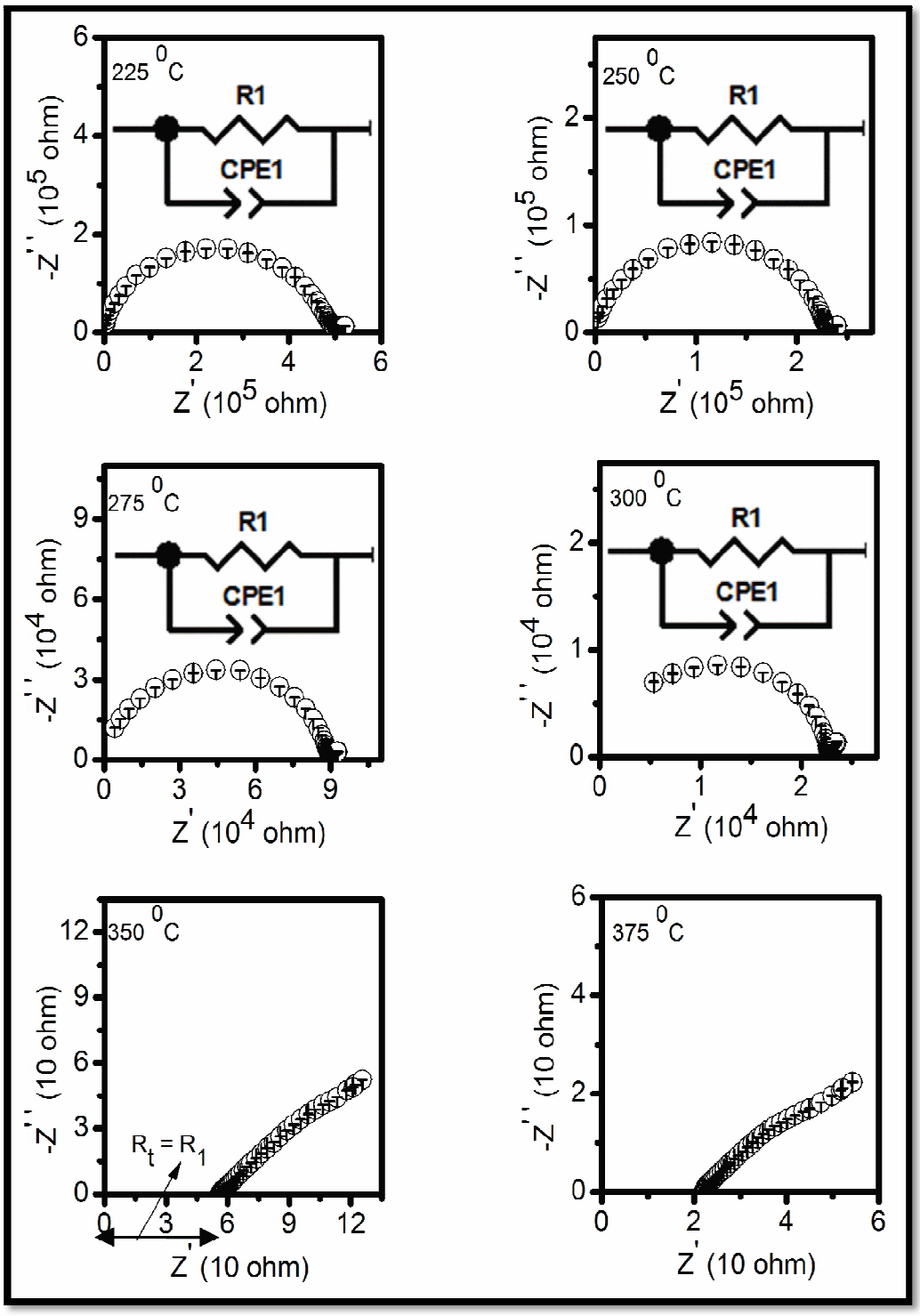

Fig. 7.17 Complex plane impedance plots of the composition CC5S2/30LNCO at different temperatures

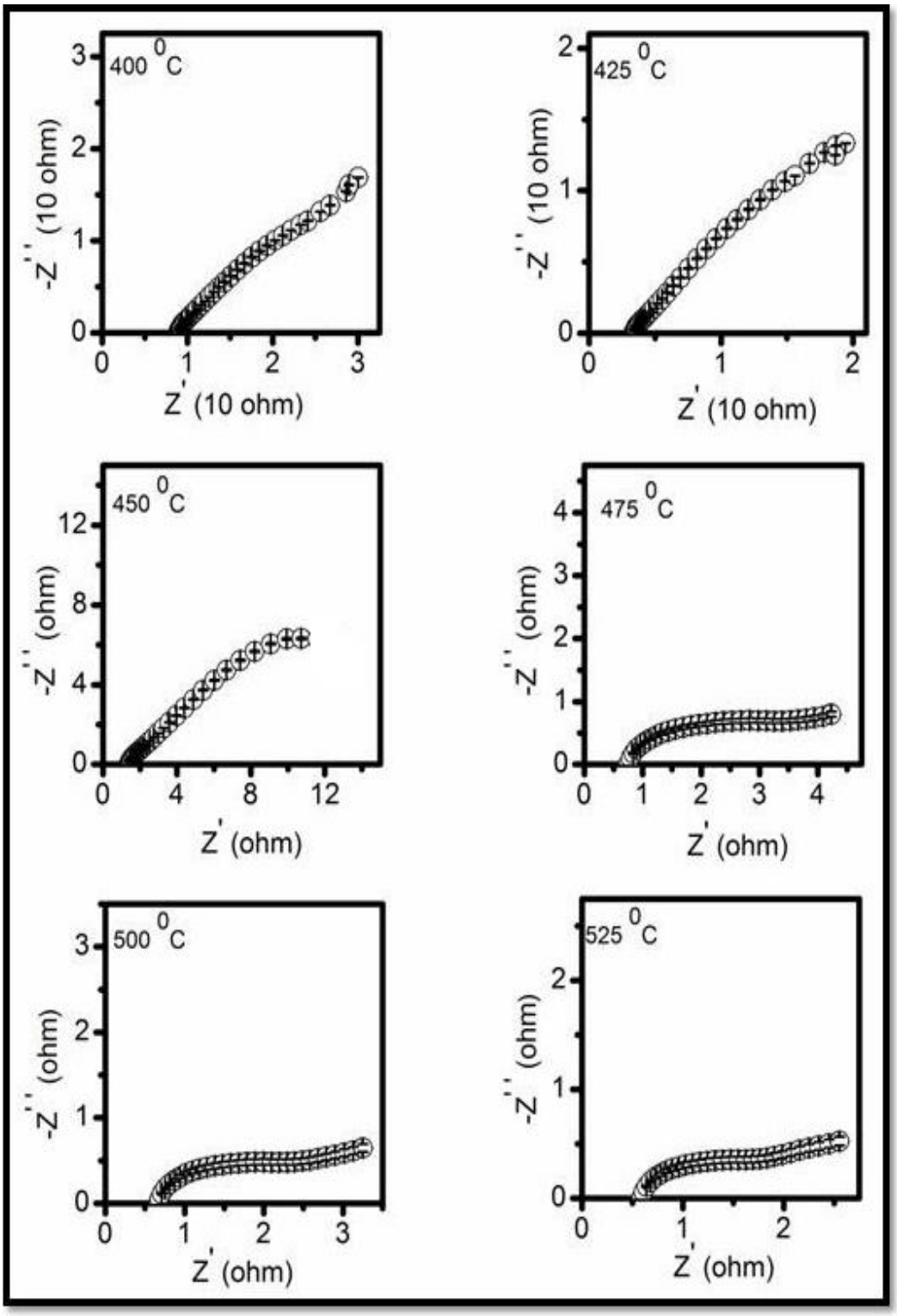

Fig. 7.17 Complex plane impedance plots of the composition CC5S2/30LNCO at different temperatures

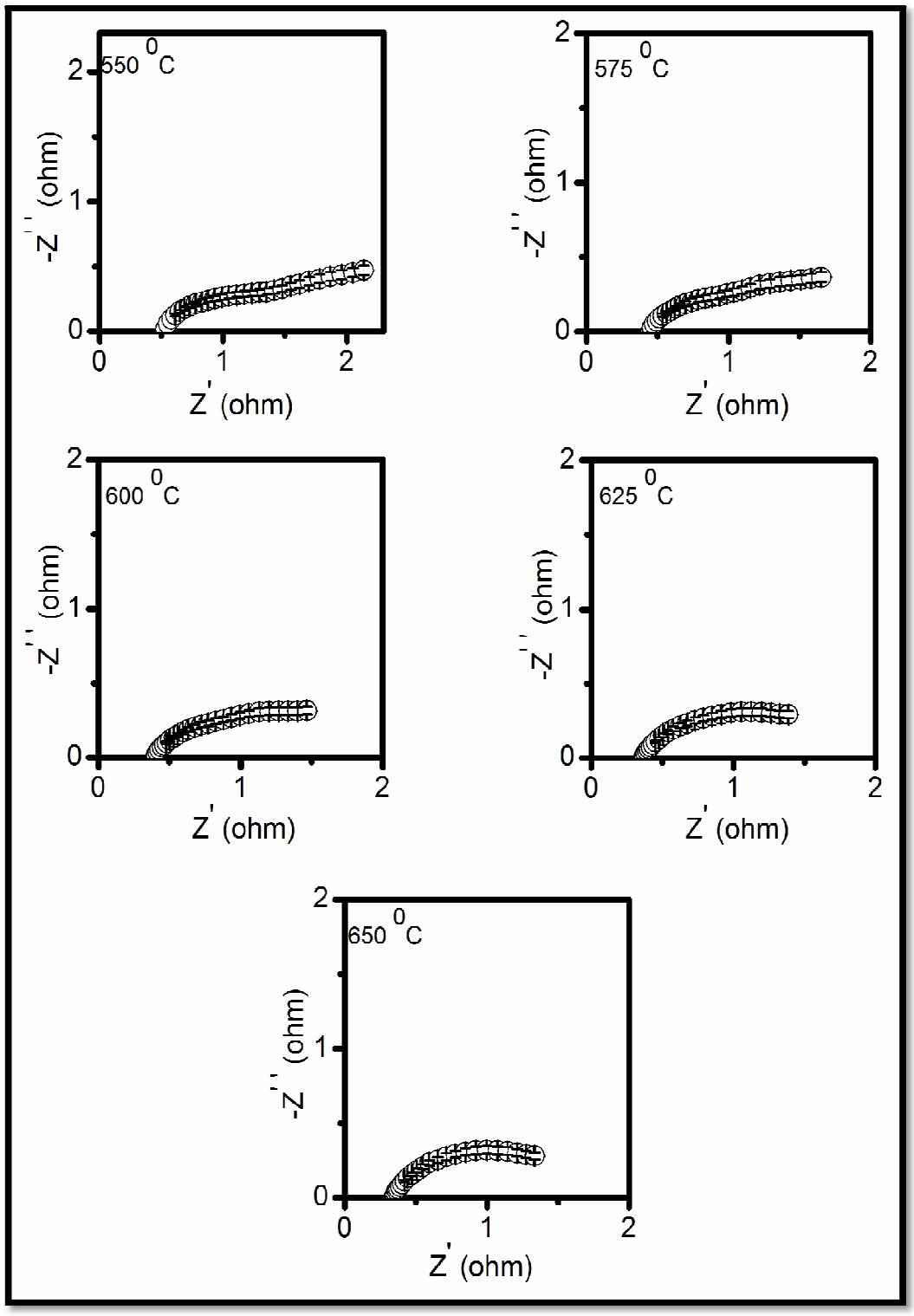

Fig. 7.17 Complex plane impedance plots of the composition CC5S2/30LNCO at different temperatures

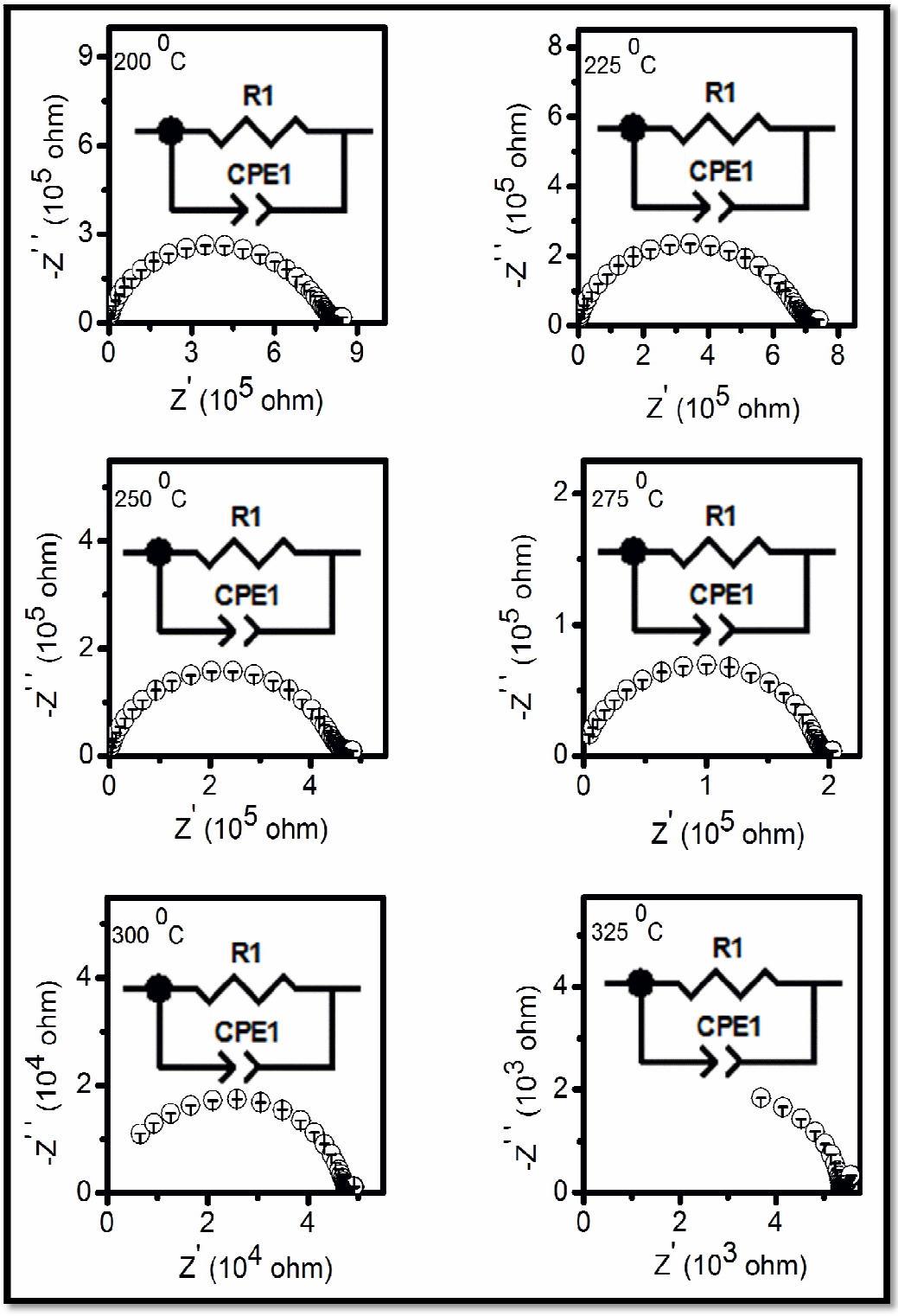

Fig. 7.18 Complex plane impedance plots of the composition CC5S2/35LNCO at different temperatures

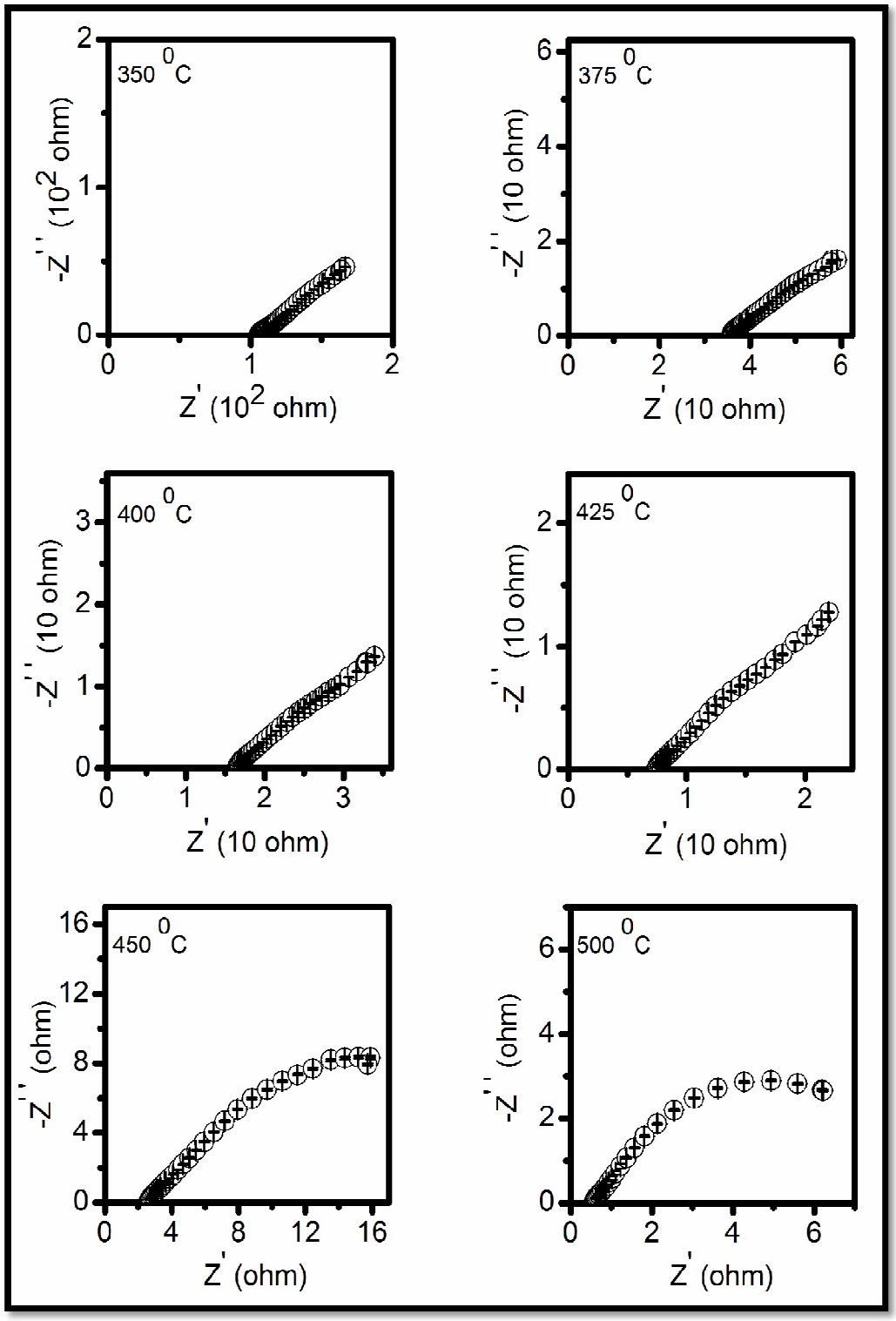

Fig. 7.18 Complex plane impedance plots of the composition CC5S2/35LNCO at different temperatures

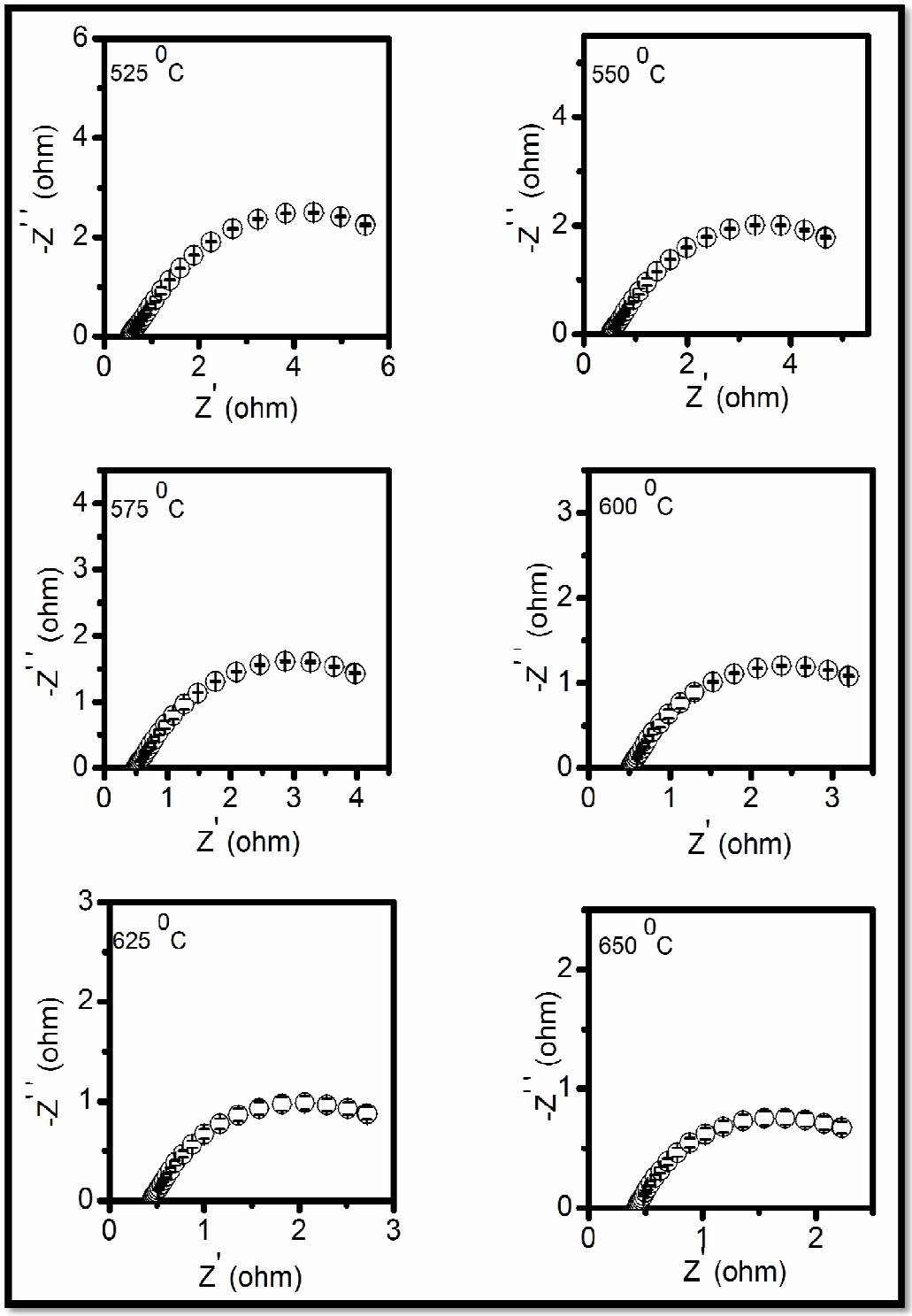

Fig. 7.18 Complex plane impedance plots of the composition CC5S2/35LNCO at different temperatures

Arrhenius plots for the total ionic conductivity of all the composites along with those of CC5S2 and LNCO are shown in Fig. 7.19. A sudden increase in the conductivity has been observed in all the composites around 350 °C. This is attributed to a superionic transition at the interface due to interfacial interaction between the ceria and carbonate phases. This forms highways for conduction of the ions. The transition temperature is certainly below the melting point of the carbonates. The possible reason for lowering of the transition temperature is the interaction of ceria and carbonate phases. This leads to the threshold percolation to form a highly conducting continuous path at the interfaces below the melting temperature of the carbonates. At the interfaces, concentration of the mobile charge carrier (Li^+, Na^+, O^{2-} and CO_3^{2-}) is higher than that in the bulk due to melting from the sublattice to the bulk [Chen et al. (2014)].

Below the transition temperature, conductivity of the composites is less than that of CC5S2. Above the transition temperature, conductivity of the composites is more than that of CC5S2 and LNOC and increases with increasing the carbonate content. In the present work, composites containing >35 wt% LNCO have not been studied because the sample containing higher concentration of carbonate are de-shaped after sintering due to large volume of the liquid formed. This has also been reported earlier [Huang et al. (2007)]. Below the transition temperature, motion of the mobile charge carriers is blocked by the solid amorphous carbonate phase. This results in less value of ionic conductivity while at higher temperature carbonates melts and fill in the gaps, creating more continuous conducting paths for the transport of the ions.

Composition, CC5S2/35LNCO shows the conductivity of 0.27 S/cm at 500 °C which is much higher than the value of 3.97×10^{-3} S/cm found in CC5S2 at the same temperature. This value is also higher than 0.01 S/cm reported for $Ce_{0.8}Sm_{0.1}Nd_{0.1}O_{1.9}/(Li/Na)_2CO_3$ by Liu et al. at 481 ºC [Liu et al. (2010)].

Activation energy (E_a) has been determined from the slope of Arrhenius plots in the low as well as high temperatures region. Activation energy is more at low temperatures and less at high temperatures. At low temperatures, diffusion of ions is being blocked by the solid carbonate phase leading to high value of activation energy.

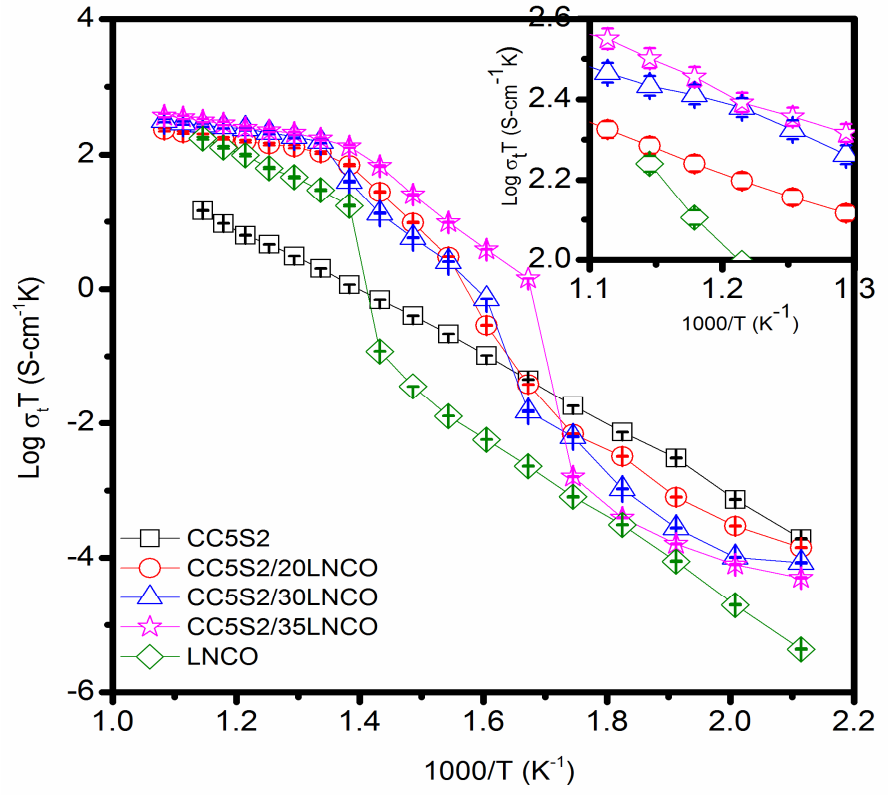

Fig. 7.19 Arrhenius plots for total ionic conductivity in the system CC5S2/LNCO

Table. 7.5 Total conductivity (σ_t) at 500 °C, activation energy (E_a) and pre-exponential factor (σ_0)

S. No.	Compositions	σ_t (S-cm^{-1}) at 500 °C	E_a <350 °C (eV)	E_a >350 °C (eV)	σ_0
1.	CC5S2	3.97×10^{-3}	0.97 (200-600 °C)		4.89×10^{6}
2.	LNCO	4.73×10^{-2}	1.26 (<500 °C)	0.30 (>500 °C)	3.05×10^{6}
3.	CC5S2/20LNCO	1.70×10^{-1}	1.44	0.25	6.76×10^{10}
4.	CC5S2/30LNCO	2.00×10^{-1}	1.75	0.20	3.63×10^{12}
5.	CC5S2/35LNCO	2.70×10^{-1}	1.77	0.30	1.40×10^{12}

The values of activation energy are given in Table. 7.5. Pre-exponential factor, σ_0 which determines the concentration of charge carriers has been calculated from the intercept of Arrhenius plots and the values are given in Table. 7.5. It is noted that composites show the higher values of σ_0 than that of CC5S2 and LNCO. This confirms that composites have large number of mobile ions and long jump distance at the interfaces. Archie plot of the system CC5S2/LNCO is shown in Fig. 7.20. It is observed that the variation of electrical conductivity with the carbonate content is non linear in the system CC5S2/LNCO.

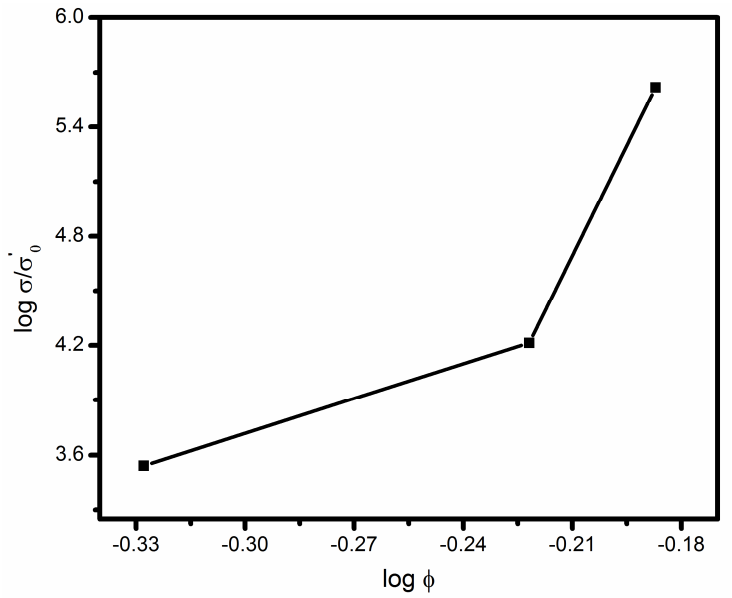

Fig. 7.20 Archie plot for the system CC5S2/LNCO

It is, therefore, concluded that conductivity of CC5S2/LNCO nanocomposites increases due to two reasons: (i) co-doping of Ca^{2+} and Sr^{2+} in ceria enhances the total conductivity as discussed above in the section 1 and (ii) molten carbonates form a uniform continuous path throughout the ceria matrix and hence create highways for the conduction of the ions. A large number of mobile ions in the space charge zone and long jump distances at the interfaces results in higher ionic conductivity and less activation energy. Composition CC5S2/35LNCO shows the highest conductivity (0.27 S/cm at 500 °C) among the samples investigated and this value is also more than the value 0.0184 S/cm at 550 °C of SDC/20LNCO reported by Fan et al. (2012).

The cost of alkaline earth oxides is much less than that of rare earth oxides. Therefore, this electrolyte may be a potential candidate for LT-SOFCs.

7.2.3 Conclusion

- Nanocomposites of CC5S2 and LNCO have been prepared successfully as the solid electrolytes for LT-SOFCs.
- In the composites, carbonates are present as an amorphous phase.
- Micrographs show that the ceria grains are fully covered by the carbonate phase consisting of a percolating network. This morphology provides more conducting paths for transport of the ions.
- Impedance analysis shows that the charge transport in the composites is different from that in the single phase ceria based electrolytes.
- A superionic phase transition has been observed in all the composites around 350 °C. Conductivity of the composites is less below the transition temperature and more above the transition temperature than the co-doped ceria.
- The composition, CC5S2/35LNCO shows the highest conductivity of all the compositions.